Journal of Materials Chemistry A

Additive Manufacturing with Stimuli-Responsive Materials

Journal:	*Journal of Materials Chemistry A*
Manuscript ID	TA-REV-08-2018-007716.R1
Article Type:	Review Article
Date Submitted by the Author:	04-Oct-2018
Complete List of Authors:	Boydston, Andrew; University of Washington, Chemistry; University Of Wisconsin Colleges, Chemistry Cao, Bo; University of Washington, Chemistry Nelson, Alshakim; University of Washington, Chemistry Ono, Robert; University of Washington, Chemistry Saha, Abhijit; University of Washington, Chemistry Schwartz, Johanna; University of Washington, Chemistry; University Of Wisconsin Colleges, Department of Chemistry Thrasher, Carl; University of Washington, Chemistry

Journal Name

ARTICLE

Additive Manufacturing with Stimuli-Responsive Materials

A. J. Boydston,[a] B. Cao,[a] A. Nelson,[a] R. J. Ono,[a] A. Saha,[a] J. J. Schwartz,[a] and C. J. Thrasher[a]

Received 00th January 20xx,
Accepted 00th January 20xx

DOI: 10.1039/x0xx00000x

www.rsc.org/

Additive manufacturing, commonly referred to as 3D printing (3DP), has ushered in a new era of advanced manufacturing that is seemingly limited only by imagination. In actuality, the fullest potentials of 3DP can only be realized through innovative breakthroughs in printing technologies and build materials. Whereas equipment for 3DP has experienced considerable development, molecular-scale programming of function, adaptivity, and responsiveness in 3DP is burgeoning. This review aims to summarize the state-of-the-art in stimuli-responsive materials that are being explored in 3DP. First, we discuss stimuli-responsiveness as it is used to enable 3DP. This highlights the diverse ways in which molecular structure and reactivity dictate energy transduction that in turn enables 3D processability. Second, we summarize efforts that have demonstrated the use of 3DP to create materials, devices, and systems that are in their final stage stimuli-responsive. This section encourages the artistic license of advanced manufacturing to be applied toward leveraging, or enhancing, energy transduction to impart device function across multiple length scales.

Introduction

Additive manufacturing (AM) has made significant advances as a field of research since its initial commercialization in the 1980s.[1] What separates AM from other manufacturing techniques is the objects are created through a build-up, or additive, process in a layer-by-layer fashion. Traditional processes often subtract or mold material into the desired shape. AM enables the ability to directly manufacture an object from a computer-aided design (CAD) file. Importantly, modifications to digital objects are facile and readily translated into iterated manufactured parts through AM. In contrast, traditional manufacturing approaches, such as injection molding, require unique tools or molds for each modification. Hence, the frequent use of "rapid prototyping" as a synonym to AM.[2] With the advent of AM also comes the ability to print complex geometries and designs that are not possible through other manufacturing methods. This includes designs such as hollow objects, lattice frameworks, graded materials, and multi-material structures.[3] The speed, versatility, and capability of advanced AM techniques have expanded its uses beyond simple prototyping and many consider it "the third industrial revolution."[4]

AM has seen remarkable engineering advancements, expanding not only the machinery and methods capable of producing objects, but also the materials capable of being processed.[5-8] Through the use of stimuli such as heat, light, and pressure, a number of additive manufacturing processes have been developed to process materials not readily accessible in other manufacturing methods. One area of ongoing growth in the AM field is the incorporation of smart, functional, and high-performance materials, which is critical to the advancement of the field. One critical area that has seen recent growth in the AM field is that of stimuli-responsive materials. Stimuli-responsive materials change their properties upon exposure to one or more stimuli such as heat, light, pH change, mechanical input, electrical input, chemical input, or magnetic input. The potential to couple the geometric freedom of AM with complex stimuli-responsive and functional materials could create any number of potential applications and advancements not possible through other manufacturing methods in fields like sensor fabrication, soft robotics, and drug delivery.[9-18] This review focuses on these advancements in terms of the intersect between stimuli-responsive materials and AM.

Our review is separated into three main sections: AM enabled by a single stimuli response, AM enabled by multi-stimuli-responsive materials, and the production of stimuli-responsive constructs by AM. The first two sections of this review discuss how the input of energy in forms such as heat, pressure, and light enable AM processes such as melt material extrusion (MME), material extrusion (ME), photojetting, and vat photopolymerization. The final section discusses how stimuli responses unleashed *after* the AM process further enables access to devices for applications such as wearable electronics, self-healing materials, drug delivery systems, and sensors. The first two sections of this review are organized according to input stimulus, such as light, heat, or pressure. The final section is sib-divided by the type of energy transduction displayed in the stimuli-response (e.g., conversion of mechanical input into chemical output).

[a] *Department of Chemistry, University of Washington, Seattle, WA 98195, USA.*
† Authors are listed alphabetically and contributed equally.

Additive Manufacturing Enabled by a Response to a Stimulus

This section focuses on AM techniques and materials that use single-stimulus-response *during* the AM process. These materials undergo a chemical or physical transformation to enable the fabrication of an object.

Light as a stimulus

Light-activated polymerization is the cornerstone of all photopolymer resin-based and ink-based AM technologies (Figure 1).[19-21] The operative mechanism that enables light-based AM involves a photosensitive liquid pre-polymer resin or ink containing photoinitiators, such as photoacid or photoradical generators. In vat photopolymerization, when irradiated with light (in a pattern-wise manner), the photoinitiators decompose and trigger polymerization and curing within the exposed region. Sequential exposure of the resin to patterned light input, along with a mechanized build plate, enables layer-by-layer fabrication of a solid, three-dimensional object. In vat photopolymerization, the ability to print a photoresin is often dictated by key material parameters such as viscosity, bulk polymerization rate, gel point, and the absorbance/refractance of the monomers and additives.[22] In photojetting, droplets of photopolymerizable ink are jetted onto a surface, and then hardened and solidified with ultraviolet light. In the context of these AM methods, light is the stimulus that triggers a chemical reaction, usually via radical formation and subsequent polymerization of reactive monomers such as acrylates, methacrylates, acrylamides, and methacrylamides. Light-based AM is different from other AM processes because the polymerization occurs *during* the manufacturing process. In contrast, other techniques use light to create a pre-formed polymeric material that is used in the AM process. The vast scope of commercially available and synthetically accessible photopolymerizable resins and monomers, the ability to modify the composition of these monomers to tailor material properties,[23,24] and the ability to print objects with sub-10 µm feature sizes makes light-based processes an attractive AM technique.[25-28]

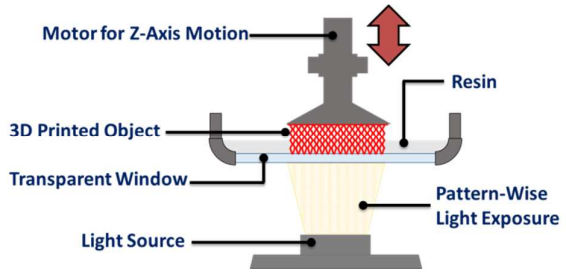

Figure 1. Schematic illustration of vat photopolymerization.

One representative example that is illustrative of recent innovations in the field of vat photopolymerization AM is the continuous liquid interface production (CLIP) process developed by DeSimone and co-workers (Figure 4a).[29] The advancement beyond a traditional stereolithographic vat photopolymerization printer design was enabled by incorporating an oxygen-permeable window between the light image projection plane (i.e., the build layer) and the light source. The oxygen permeability led to the formation of a thin oxygen-rich layer of uncured liquid resin, creating a dead zone between the window and the cured surface wherein a gradient of oxygen exists. Radical polymerization is inhibited within the dead zone as a consequence of the oxygen inhibition—either by the quenching of the excited-state photoinitiator or by the formation of a peroxide interaction with a free radical of a propagating polymer chain. In CLIP, the printed polymeric object can be continuously lifted out of the resin bath as opposed to the step-wise layer-by-layer process required in traditional vat photopolymerization. This has been demonstrated to afford faster print times, objects with mechanical properties that are independent of print orientation, and a reduction in the "staircase" surface finish effect often seen in objects printed using layer-by-layer processes.[30] The critical factor for this printing method is the use of oxygen-inhibited photopolymerization mechanisms, mainly radical mediated polymerizations. Other mechanisms that are not inhibited by oxygen would not be printable in this printing method.

Another method of light-based AM that goes beyond traditional vat photopolymerization is the living additive manufacturing (living AM) demonstrated by Johnson and co-workers. In this approach, a "daughter" object was created by AM from a parent hydrogel which was produced by AM**.** This approach involved a photoredox catalyzed growth (PRCG) to spatiotemporally insert monomers such as *N*-isopropylacrylamide (NiPAAm) into dynamic covalent polymer networks of the dormant "parent" materials to generate more complex and diversely functionalized "daughter" material.[31] Photo-induced insertions of new monomers during the AM of "daughter materials" demonstrated the livingness of the AM process. A homogeneous end-linked gel bearing trithiocarbonate (TTC) iniferters within the network chains was synthesized for the PRCG. The "parent" gel was then exposed to a blue LED light in a solution containing monomer, crosslinker (N,N'-methylenebisacrylamide), and photocatalyst (10-phenylphenothiazine (PTH)). Irradiation with blue light excited the PTH and initiated photoinduced single electron transfer from PTH to the TTC to afford a TTC radical anion and the PTH radical cation. This not only stabilized the TTC anion, it further enabled the living insertion of monomers and crosslinkers from solution into the network strands following the photoredox catalysis mechanism. A wide range of chemically and mechanically differentiated daughter gels was produced by using the living AM from a single type of parent gel via light-controlled modification of the parent's average composition, strand length, and crosslinking density. Not only could this control whether the "daughter" gel was stiffer or softer than the "parent" gel, but also induce changes in stimuli responsiveness, polarity, and thermal properties while maintaining similar mechanical properties through similar crosslink densities.

One representative example of the recent innovations through photojetting technologies was developed by Qi and co-workers through multi-material printing of shape memory polymers (SMPs) to create self-folding structures.[32] Shape memory polymers are

materials that can go from a temporary programmed shape to a fixed "permanent" shape upon heating. A more detailed explanation can be found in the shape memory section within this review. By printing objects using multiple inks, Qi and co-workers were able to control the thermomechanical properties of SMP hinges within their structures and create designs that could fold controllably under uniform thermal heating environments. They were able to utilize this to make self-folding, and self-locking 2D geometries as well as a 3D box structure. The box utilized differential speeds of folding of materials printed with different ink formulations to induce programmed sequential folding to go from a flat sheet to the final 3D structure.

Heat as a stimulus

Perhaps the most widely established stimulus that enables AM is heat. [33,34] Many AM techniques such as selective laser sintering (SLS), electron beam melting (EBM), laminated object manufacturing (LOM), and MME, rely on heat as the stimulus to melt or fuse the materials. Consumer-friendly printers for MME (also known as fused deposition modelling, or FDM) can be found in both academic and industrial settings. MME printers use a thermoplastic filament that becomes pliable when heated above its glass transition temperature (T_g) or melting temperature (T_m). The heated filament is extruded in a layer-by-layer fashion until the desired 3D object is formed. To date, many thermoplastic materials have been developed into MME filaments, which vary in toughness, stiffness, and elasticity. The most common MME filaments include polylactide (PLA), acrylonitrile butadiene styrene copolymer (ABS), polycarbonate (PC), and polyurethane (PU).[35] The extruder temperature and the print bed temperature are important considerations for MME printing. The extruder temperature is typically set well above the T_g or T_m of the filament to ensure that the material is fully molten as it passes through the printer nozzle. For instance, typical print temperatures for PLA (T_m = 150-160 °C) and ABS (T_g = 105 °C) are in the range of 180-220 °C and 230-250 °C, respectively. The print bed temperature is critical in cases where the printed material is prone to contraction upon rapid cooling, which can lead to warping of the printed objects. This is typically less of an issue for PLA; however, it is well known that when printing ABS filament, the print bed must be heated to temperatures approaching the T_g of the filament (~105 °C) to avoid warping. Additionally, rapid cooling of the filament as it is extruded results in poor adhesion between layers and compromised mechanical properties.[36]

An exciting innovation within MME printing is the use of thermally-reversible dynamic covalent chemistry to form covalent network assemblies throughout printed objects. To this end, Smaldone and co-workers recently utilized thermally-reversible Diels–Alder chemistry to engineer a polymer system that thermally depolymerized during the print process followed by re-polymerization during cooling to improve the fusion at the filament interface. The interlayer strength of printed objects were improved as a result.[37] A furan-maleimide Diels–Alder network polymer was blended with commercial PLA, pelletized, and fabricated into a filament. The dynamic reaction favored the furan-maleimide adduct at low temperatures (~40– 50 °C), while at elevated temperatures (~100– 120 °C) the retro Diels-Alder reaction is favored. Objects printed using the PLA blended with the mending agent exhibited an increase in interlayer adhesion strength of up to 130% compared with those printed using the commercial PLA filament (print orientation normal to the axis of tension). During extrusion, thermoplastic PLA melted at ~100– 120 °C with a huge drop in viscosity, while the mending agent de-polymerized at that temperature. Once the extruded filament cooled down, the Diels-Alder reaction favored the re-polymerization of the mending agent. This allowed the molecular level interlayer crosslinking of the extruded filaments at their junctions. The toughness of the z-axis aligned prints increased by up to 1150% for the blended PLA compared to unmodified PLA as a result of the increased crosslinking density.[38] Through further improvement of their reversible thermosetting filaments, Smaldone and co-workers were able to achieve printed objects that had greater than 95% interlayer adhesion. Generally, objects printed through melt material extrusion exhibit a large anisotropy in mechanical properties when comparing strength and toughness along the axes of material deposition (often x and y) versus across multiple layers of deposition (often the z axis). Because of the formation of interlayer reversible furan-maleimide Diels–Alder linkages bonds, and thereby high interlayer adhesion, the toughest materials exhibited baseline toughness of 18.59 ± 0.91 and 18.36 ± 0.57 MJ m^{-3} perpendicular (x-axis) and parallel (z-axis) to the build direction, respectively. This interlayer adhesion not only led to isotropic mechanical properties but also resulted in more visually appealing MME objects because the individual layers were indistinguishable.[39]

Pressure as a stimulus

Polymeric hydrogels are often used as inks for the fabrication of 3D patterns via direct-write printing.[40-43] This type of printing is similar to MME in that a nozzle travels across a surface in a pattern-wise manner to afford multi-layered objects, but the material is extruded at ambient temperatures with the use of pressure. The hydrogel inks used for this type of printing are typically shear-thinning—the viscoelastic properties of the gel change based on the pressure exerted onto the gel. The viscosity of a shear-thinning hydrogel decreases under pressure as the material passes through the nozzle, but then the gel rapidly recovers its original modulus after exiting the nozzle, as the pressure is immediately removed, to maintain its extruded shape (Figure 2).

A combination of self-assembly, and physical crosslinking of polymer networks is responsible for the formation of shear-thinning hydrogels. The breaking of physical crosslinks under high-shear and their instantaneous recovery under shear-relaxed environments gives rise to the reversible self-healing nature of the hydrogels. Rheological measurements are useful to explore the 'printability' of hydrogel materials via ME.[44] The printability of a hydrogel relates to a number of factors,

including pressure, viscosity, flow rate, shear recovery time, and the extent of reversibility in the making and breaking of crosslinks during shear thinning.[45] The gel yield stress correlates with the force required to extrude the gel through the nozzle and provides an indication of the ability of the gel to support stacked layers. The shear-thinning ability of a hydrogel, that is, its tendency to decrease its viscosity with increasing shear strain, is also evaluated as this enables the gel to lower its viscosity to flow as a liquid as it is extruded through a small diameter nozzle. The ability to quickly recover its viscoelastic moduli under the shear-relaxed environment immediately following extrusion (i.e., its reversible self-healing behavior) is an important characteristic for hydrogels used in ME for fidelity and integrity of the objects. The reversible shear-thinning under stress and rapid recovery of the modulus under shear-relaxed conditions can be evaluated on a rheometer by conducting cyclic shear-thinning experiments. Therefore, the rheological assessment of the shear-thinning hydrogels to characterize the yield stress, shear-thinning and modulus recovery behaviours evaluates the suitability of the hydrogels as materials for ME.[46-48]

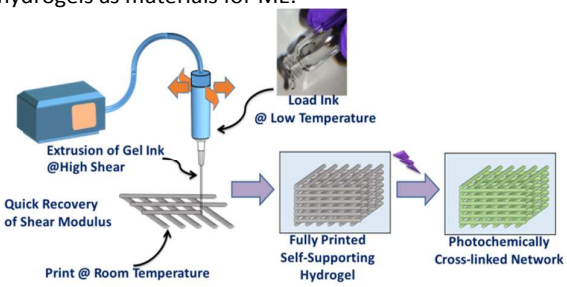

Figure 2. Schematic illustration for the heat, pressure, and light-responsive shear-thinning hydrogel inks for ME.

Lewis and co-workers reported a shear-thinning hydrogel as an ink for ME comprising a mixture of polyacrylamide (M_v = 89 kDa), acrylamide, *N*,*N*-methylene bisacrylamide, and a photoinitiator in a mixture of glycerol and water.[49] The ink was prepared by first aging a mixture of acrylamide monomer, glycerol, and water for several hours under ambient conditions, during which time, the monomeric species polymerized to yield a 30 % water-in-oil polyacrylamide gel. The resulting hydrogel had an elastic modulus of ca. 3 kPa and exhibited shear-thinning behavior. The ink was further optimized with the addition of monomer, *N*,*N*-methylene bisacrylamide, and photoinitiator to optimize the ink composition, which was used to print 3D objects that were photopolymerized in situ to prevent deformation of the printed patterns (Figure 4h). Under ambient conditions, the reversible physical crosslinking between the polyacrylamide chains helped to retain the modulus and shape of the hydrogel. But under high shear rates (~100 s^{-1}), these inter-chain interactions were broken to afford a shear-thinning behavior. Hydrogel scaffolds composed of 1–4 layers of 5-µm extruded filaments with 20-µm spacing between the extruded filaments and a total area of 5 mm^2 were printed at 0.5 mm s^{-1} print speed. This method of ME with in situ photo crosslinking was extended to AM using other materials that were suitable for tissue-engineering, such as crosslinkable hyaluronic acid, and poly(ethylene glycol) diacrylate (PEG-DA).[50,51] Mahadevan, Lewis, and co-workers further advanced the composition of the of the hydrogel ink by introducing nanofibrillated cellulose (NFC) and clay to improve shear-thinning and swelling behaviors of the hydrogels.[52] Synthetic hectorite clay, Laponite XLG, enables polymerization to initiate from the surface on the clay due to the high cationic exchange capacity of the clay. The clay being a strong physical, multifunctional crosslinker afforded high stretchability and strength compared to covalently crosslinked hydrogels without clay. The composite viscoelastic ink comprised of an aqueous solution of *N*,*N*-dimethylacrylamide (or NiPAAm for reversible systems), photoinitiator, nanoclay, glucose oxidase, glucose, and NFC. Each component of the hydrogel ink served a particular purpose: 1) the clay particles were a rheological aid that afforded the viscoelastic behavior required for ME, 2) glucose oxidase and glucose minimized oxygen inhibition during the ultraviolet (UV) curing process by scavenging ambient oxygen, and 3) NFC with high aspect ratio (~100), served as stiff fillers (elastic modulus > 100 GPa). After ME, the acrylamide monomer was photopolymerized and physically crosslinked by the nanoclay particles, producing a biocompatible hydrogel matrix that swelled readily in water. During ME, the NFCs experienced shear-induced alignment as the ink flows through the deposition nozzle, which led to extruded filaments with anisotropic stiffness, and hence, swelling behavior in the longitudinal direction (along the length of the filament), as opposed to the transverse direction (Figure 4d). As a result, swelling induced change in the shape of 3D objects were observed.

Other stimuli or factors enabling printing

Supramolecular interactions such as ionic and host-guest complexations have also been used to enable ME. For example, the ionic interaction between calcium ions and the carboxylate groups of alginate has been used as a method to crosslink 3D printed hydrogels. Gelinsky and co-workers used an alginate/methylcellulose blend (1:3 w/w) in water as an ink for ME.[53] After extrusion, incubation of the printed scaffold in a solution of $CaCl_2$ for ten minutes was sufficient to obtain an ionically crosslinked Ca^{2+}/alginate network (Figure 4c). This printing method circumvents the need for UV-curing and is a very promising AM technique for embedding living cells under milder conditions.

Another example of work that harnesses chemical stimuli to enable printing was demonstrated by Burdick and co-workers in supramolecular host-guest complexation between adamantane (Ad) and β-cyclodextrin (β-CD).[54] This complexation was exploited to develop shear-thinning hydrogels as an ink for ME. Under high shear, the dynamic noncovalent and reversible host-guest complex disassociated, which allowed the hydrogel to shear-thin. Instantaneous reformation of the host-guest complex after extrusion, from the decrease in pressure, enables the rapid self-healing of the extruded hydrogels. The hydrogels were composed of

hyaluronic acid (HA) chemically modified with either Ad or β-CD, denoted as Ad–HA and CD-HA, respectively. Upon mixing of Ad–HA and CD–HA in a 1:1 ratio, the host-guest complexation induced crosslinking in the gels. In order to enable ME, a gel-in-gel printing method was devised. The extruded ink was comprised of a 1:1 mixture of Ad-HA and CD-HA adjusted to 5 w/v% was used, wherein 25% of the repeat units on both sets of polymers were modified. The support gel was comprised of a 4 w/v% 1:1 mixture of Ad-HA and CD-HA, where 40% of the respective repeat units were functionalized. Rheological examination revealed that there was an increase in material stability in the hydrogel (i.e., loss of bulk relaxation behavior) with the increase in the number of complexation sites. The dynamic nature of these complexes afforded hydrogel inks that could self-heal, which is an important aspect of the success of these materials. The viscoelastic properties of the hydrogel ink enabled extrusion through needles of varied diameters and maintained print fidelity after dispensation into the support matrix. When a syringe needle was inserted to inject the hydrogel ink, the support gel deformed but rapidly self-healed around the printed ink. Gels that contained an HA backbone with higher degrees of chemical modification with the guest (Ad) or host (β-CD) moieties, as much as 40% of the backbone, showed superior viscoelastic properties. Additionally, Burdick and co-workers introduced methacrylate functionalities onto HA (ca. 20% of repeat units) to enable photoinitiated secondary covalent crosslinking to afford a dual crosslinked network. This strategy has been further developed to include RGD peptide functionalization of the HA to support cell adhesion which is useful for tissue engineering applications.[50]

While the previous example demonstrated a hydrogel ink that can be seeded with cells after printing, Heilshorn and co-workers demonstrated ME using a cell-laden ink.[55] Alginate was modified with either ~10 proline-rich peptide domains or with a complementary recombinant engineered protein (termed C7). These two alginates were used to develop the two components of a hydrogel bioink. The first stage of crosslinking relied on the mixing of the two-components with the molecular recognition between the complementary peptide-binding domains designed into each component. This step was referred to as Mixing-Induced Two-Component Hydrogel, or MITCH. Upon mixing, the complementary domains self-assembled, forming physical crosslinks between the two components to create a weak hydrogel network. Rapid shear-thinning and self-healing behavior of hydrogel was observed after the first stage of crosslinking. The second stage involved the ionic crosslinking between calcium ions in solution and the alginate backbone with a 100-fold increase in modulus after exposure to calcium ions. An advantage of this approach is that MITCH afforded a hydrogel that not only prevented cell sedimentation, but also provided significant mechanical protection from membrane damage during extrusion. The ionic crosslinking via the formation of calcium alginate complexes is necessary to provide the printed structure with mechanical support. This dual-stage hydrogel bioink avoids the use of any covalent crosslinking, which could be advantageous for creating synthetic tissue scaffolds.

Additive Manufacturing Enabled by Multi-Stimuli-Responsive Materials

While we have, thus far, discussed the role of single-stimulus responsive inks for enabling AM, multi-stimuli-responsive materials have also been developed. Orthogonal stimuli responses can be employed to produce the printed inks or to improve the quality of the printed product. Indeed, several stimuli responses go hand-in-hand when it comes to the AM process. For instance, while a shear-thinning behaviour can be critical for ME processes, the addition of a temperature-responsive feature to the hydrogel ink can also be advantageous (Figure 2). A thermo-reversible hydrogel that exhibits a characteristic 'sol-to-gel' transition temperature (T_{gel}) can be handled in its 'sol' state to incorporate additives (such as nanomaterials or living cells) homogeneously or to load the printer ink cartridge; in its 'gel' state, the same hydrogel ink can be printed with a direct-write printer.

Two representative materials that exhibit this type of temperature-responsive behavior are F127 and gelatin-methacrylamide (GelMA) hydrogels. Both of these materials are thermoreversible gelators, albeit with inversed behaviors.[56] Commercially available F127 is a triblock copolymer that consists of a central hydrophobic poly(propylene oxide) (PPO) block flanked by two hydrophilic poly(ethylene oxide) (PEO) blocks. Concentrated aqueous solutions of F127 reversibly form liquids at low temperatures and gels at higher temperatures, whereas GelMA solutions are gels at low temperatures and liquids at higher temperatures. The thermoreversible gelation of F127-based hydrogels is primarily driven by the lower critical solution temperature (LCST) of the PPO block. Below 5 °C, the polymer molecules are soluble in water and exist as soluble unimers to afford a viscous solution. As the temperature is increased, the solubility of PPO in water decreases, driving the formation of micelles consisting of PPO cores surrounded by PEO coronas, resulting in the gel state.[57] Depending upon the polymer concentration, the values for the T_{gel} of F127, a widely-used and commercially available composition of Pluronic™, and GelMA fall within the range of 15-20 °C and 32-35 °C, respectively, making those useful for ME printing at room temperature.

The Lewis group has utilized the dual stimuli-responsive nature of F127 to develop a unique gel-in-gel ME printing method known as "omnidirectional printing" (ODP).[58] The authors used F127 (23 wt%) and diacrylated F127 (F127-DA; 25 wt%) hydrogels as a fugitive ink and reservoir matrix, respectively, to print 3D biomimetic microvascular networks. A 20 wt% F127-DA solution was used as filler fluid and was poured on top of the reservoir matrix. Above the critical micelle concentration (CMC) of F127, the micellar network produces gels by physical crosslinking, which is accompanied by a substantial increase in the material's shear elastic modulus (G'). The fugitive ink and reservoir matrix hydrogels

exhibited noticeable shear-thinning behavior, which allowed the ink to be extruded through the nozzle. Rapid recovery of the G' under a shear-relaxed state (i.e., immediately following extrusion) allowed the hydrogel to maintain the filament form. The G' of the reservoir gel (F127-DA) supported the deposited filaments without disruption due to viscous drag as the nozzle travelled through the gel matrix. Subsequently, the filler fluid at concentration below the CMC quickly flowed in to fill the void spaces generated locally due to the movement of the nozzle. Upon fixing the F127-DA gel reservoir by photopolymerization, the entire structure was cooled down to liquefy and remove the fugitive F127 gel ink, to reveal a microvascular network. Following up on this work, the Lewis group printed both F127 and GelMA within a single reservoir matrix using the gel-in-gel printing technique to create vascularized, heterogeneous cell-laden tissue constructs.[59] These complex structures would not be possible in ME methods that do not utilize support systems.

Feinberg and co-workers developed a different, novel gel-in-gel printing method utilizing the thermo-reversible properties of gelatin to print soft and delicate objects that would be challenging to create using traditional approaches.[60] The technique, which the authors termed freeform reversible embedding of suspended hydrogels (FRESH), involves the use of a thermo-reversible support bath comprised of gelatin microparticles into which a low modulus hydrogel is deposited in 3D space. The gelatin support bath acts like a Bingham plastic during the printing process, allowing for the print nozzle to move through the bath with little mechanical resistance, while simultaneously maintaining the structural integrity of the printed material and holding it in place (Figure 4g). Upon completion of the printed structure, the bath was heated to 37 °C (above the T_{gel} of the material), which caused the gelatin bath to melt without destroying the printed object. Using this technique, the authors successfully printed several objects resembling complex biological structures based on medical CT and MRI data, including a miniaturized human femur, a coronary arterial tree, and an embryonic chicken heart, out of sodium alginate hydrogels. Other hydrated biomaterial inks that were found to be compatible with the FRESH printing process included fibrin, collagen type I, and Matrigel.

Nelson and co-workers demonstrated a method to print robust hydrogels and hydrogel composites via gel-in-gel direct-write printing of a catalytically activated polymerization to induce crosslinking.[61] A polymerizable shear-thinning hydrogel ink of dimethacrylated F127 (F127-DMA) with tetramethylethylenediamine as catalyst was directly extruded into a shear-thinning hydrogel support bath of F127 with ammonium persulfate as initiator in a pattern-wise manner. This gel-in-gel ME enabled the fabrication of robust spanning or overhanging structures. Without the underlying support gel, structures tend to sag or collapse (Figure 4b). When the two gels came into contact, the free radicals generated by the catalyst initiated the polymerization of the hydrogel ink. The catalyst-initiated polymerization is particularly useful for printing opaque hydrogel inks which depends upon light penetration through the sample to enable the curing step. The ink gel and support bath hydrogel exhibited a temperature-responsive behavior in which the gel transitioned into its 'sol' state upon cooling below 16 °C. This feature allowed the facile removal of the printed structure from the support bath. Hydrogel composites with graphene oxide (GO) and multiwalled carbon nanotubes (MWCNTs), which are difficult to print with photocrosslinking print methods, were successfully printed using this process.

Utilizing the multi-stimuli-responsive F127-DMA hydrogels, Nelson and co-worked further developed living materials which they referred to as "additive manufactured catalytically active living materials (AMCALMs)."[62] Using a *Saccharomyces cerevisiae*-laden 25 wt% F127-DMA hydrogel ink enabled the fabrication of 3D constructs based on a computer aided design (CAD) model. The temperature-dependent gelation behavior of the hydrogel was ideal for homogeneously incorporating yeast cells at 5 °C that then afforded a uniform distribution of cells in the gel at room temperature. The yeast-embedded AM living materials were viable and metabolically active in the fermentation of glucose into ethanol for 2 weeks in a continuous batch process without significant reduction in efficiency (~90% yield of ethanol).

Bioprinting for tissue engineering has also been demonstrated using multi-stimuli-responsive hydrogels. Zenobi-Wong and co-workers used a mixture of F127 and F127-DA as the ink for 3D bioprinting (Figure 4f).[63] At 37 °C a 20 w/w% polymer blend (2-3% of F127-DA) in water formed a hydrogel. Rheological measurements of the hydrogel at 37 °C showed excellent shear-thinning and shear recovery properties desirable for direct-write printing. The dependence of shear rate on viscosity (~11 kPa s) was observed even at a very low shear rate (10^{-2} s^{-1}), while at very high shear rates (100 s^{-1}) the viscosity dropped below 3.5 Pa s, thus enabling the ink to flow through the nozzle. The gel showed quick recovery of elastic modulus under shear-relaxed conditions as well as thixotropic behavior. Elusion of F127 from the ME structures after photo crosslinking over time led to a more porous hydrogel network and it was termed as "nanostructuring". To assess the effect of this nanostructuring on cell viability, Zenobi and coworkers printed cell-laden gels and conducted cell viability assays. Chondrocytes were used and were obtained from a bovine femur. For the viability assays and printing, passage 4 bovine chondrocytes were encapsulated in the nanostructured Pluronic hydrogels at a concentration of 2×10^7 cells/ml. Nanostructuring had positive influence on the viability of encapsulated bovine chondrocytes in the 3D printed hydrogels. Cell viability of encapsulated chondrocytes at day 14 had shown significant improvement from 62% for a pure acrylated Pluronic hydrogel to 86% for a nanostructured hydrogel with an initial 3% of F127DA.

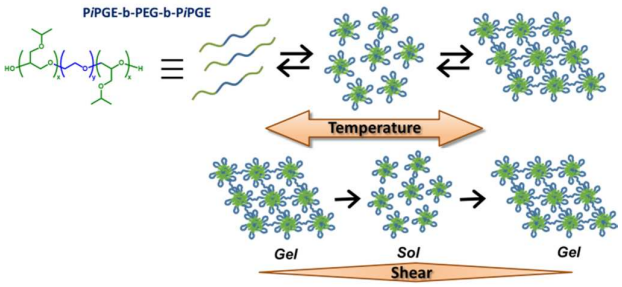

Figure 3. Cartoon representation of the temperature and shear response of hydrogels of alkyl glycidyl ether (PiPrGE-b-PEG-b-PiPrGE). Reprinted with permission ref. 64. Copyright (2015) American Chemical Society.

Nelson and co-workers recently reported a dual-stimuli-responsive triblock copolymer, poly(isopropyl glycidyl ether)-*block*-poly(ethylene glycol)-*block*-poly(isopropyl glycidyl ether) (PiPrGE-*b*-PEG-*b*-PiPrGE) that afford shear responsive hydrogels for direct-write printing (Figure 3).[64] These polymers are BAB triblock copolymers with thermo-responsive 'B' blocks and a hydrophilic 'A' block (in contrast to F127 which has an ABA architecture). The polymers displayed reversible self-assembly and micelle-forming behavior similar to F127 but exhibited superior performance to the latter with respect to its thermal and shear response. The PiPrGE-*b*-PEG-*b*-PiPrGE formed gels at considerably lower polymer concentrations than that of the F127 gels at 25 °C. The authors conducted a suite of rheological experiments to compare the viscoelastic properties of the hydrogels derived from PiPrGE-*b*-PEG-*b*-PiPrGE to that of F127, and also correlated the rheological behavior with the 3D printing performance. The equilibrium elastic moduli for the gels were on the order of 10^4 Pa and the gel yield stresses were much higher than that of F127. This indicated that the former were stronger gels that could better support their own weight during the 3D printing of stacked layer structures. A decrease in the viscosity of the gels with increasing shear rates was indicative of shear-thinning behavior. Rapid recovery of the elastic modulus was observed under shear relaxed environments, and the hydrogel could be repeatedly subjected to several consecutive cycles of high and low strain without hysteresis, thus revealing the reversible self-healing nature of the gels. A resolution of 100 µm could be achieved with ME printed structures. Notably, vertically oriented pillar structures up to 2400 µm tall could be printed with PiPrGE-*b*-PEG-*b*-PiPrGE whereas similar structures printed with F127 hydrogel collapsed. Nelson and co-workers further developed a series of triblock copolymers hydrogels that responded to temperature and pressure (shear-thinning) and were also capable of crosslinking upon its exposure to 365 nm UV light. After printing the gel using a direct-write printer, the light response facilitated the crosslinking of the polymer chains to afford robust 3D objects. The moduli of 3D objects were also tuned by varying the UV-exposure time.[65]

Dubruel and co-workers explored the 3D printing of HepG2 cell-laden GelMA hydrogels using a direct-write printer.[66] The authors conducted a systematic study of various parameters affecting printing, including the choice of photoinitiator, hydrogel concentration, printing temperature, and nozzle type. Based on their temperature-dependent rheological data, the authors determined that it was necessary to 1) apply a jacketed temperature control unit to the dispensing needle tip and 2) attach Peltier elements to the stainless-steel build platform in order to enable cooling. Cooling of both the dispensing needle and the build platform was necessary to ensure that the GelMA cell-laden ink remained in the gel form, which was crucial for maintaining mechanical integrity of the gels, especially for plotting multi-layered structures. The printed structure could then be crosslinked upon exposure to UV irradiation.

Shah and co-workers presented a multi-material formulation approach toward preparation of cell-compatible, printable gel-phase bioinks that took advantage of both the pressure- and light-responsive behaviors of the ink.[67] To formulate the bioinks, natural or synthetic polymers that present amine functional groups (e.g., gelatin, GelMA, PEG diamine) were mixed with a reactive homobifunctional linear or 4-armed PEG crosslinker containing succinimidyl valerate (SVA)

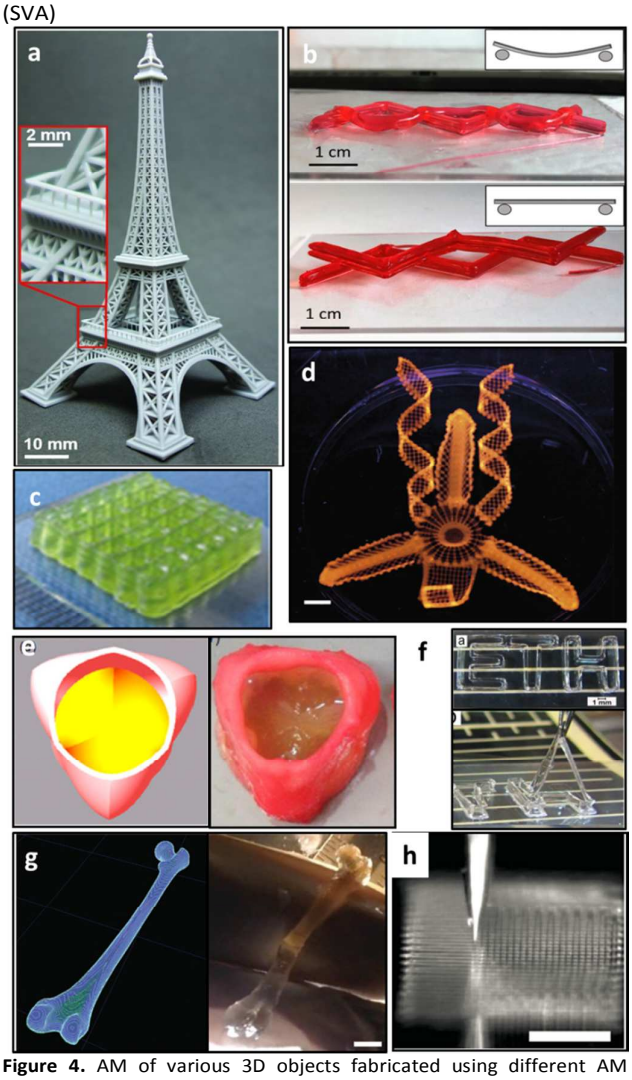

Figure 4. AM of various 3D objects fabricated using different AM

techniques a) Eiffel Tower model, 10 cm tall fabricated using CLIP printed at a rate of 100 mm/hour (inset of 1. Shows where features <1 mm in size are obtained).[30] b) Side view of 3D structures without support gel (top) and with support gel (Bottom) using gel-in-gel ME showing possible deformation in absence of the support gel (inset).[61] Reprinted with permission ref. 61. Copyright (2017) American Chemical Society. c) A 20-layer algae-laden Ca^{2+}/alginate hydrogel construct fabricated using ME (area: 15 mm x 15 mm).[53] d) A swollen 3D construct in water developed inspired by a native orchid, the Dendrobium helix (AM by using bio-4DP; scale bar 5 mm).[52] Reprinted by permission from Springer Nature. e) (Left) A CAD model for the axisymmetric porcine aortic valve and (right) AM of the aortic valve with an inner diameter of 22 mm.[51] f) (Top) ME of "ETH" logo using Pluronic™ hydrogel with a line width is 700 µm (scale bar 1 mm) and after photo crosslinking (bottom) the structure becomes stiff enough to be manipulated with tweezers.[63] g) A model of a human femur from 3D CT imaging (left) and the femur (AM using FRESH in alginate) closely resembles the model (right, scale bar 10 mm).[60] h) Layer-by-layer ME and simultaneous photo crosslinking of a shear-thinning hydrogel (scale bar 200 µm).[49] Each figure has been reproduced with permission from the respective references.

end-groups to induce crosslinking via amine-carboxylic acid coupling. Adjusting the concentration, polymer molecular weights, and polymer-to-crosslinker ratio affected the rheological properties of the resulting gels. Formulations that were suitable for printing were subsequently identified and successfully printed into self-supporting structures. The authors hypothesized that the critical strain and critical stress of the gels were important rheological parameters that correlated with their 3D printability. A second, post-printing crosslinking reaction via UV irradiation could be carried out for inks that contained polymers with photopolymerizable groups (e.g., GelMA), further increasing the stability and robustness of the printed constructs. The authors noted that in addition to the amine-carboxylic acid crosslinking chemistry presented in this work, the highly tailorable strategy toward bioink formulation should be extendable toward other crosslinking chemistries, thus greatly expanding the scope of printable bioinks.

Butcher and co-workers reported a method to employ photo-crosslinking coupled with ionic crosslinking to engineer anatomically accurate aortic valve hydrogel scaffolds (Figure 4e).[51] Native aortic valve geometries were 3D printed with PBS solutions of PEG-diacrylate (PEG-DA) supplemented with alginate, the latter of which was added to increase the viscosity of the ink formulations to be suitable for extrusion printing. The 3D printer was modified to carry up to three syringes, allowing for multiple materials to be incorporated into printed objects. To print the aortic valves, the authors used two different gel inks: first, a mechanically stiff gel comprising 20% w/v 700 MW PEG-DA and 12.5% w/v alginate in PBS, and second, a compliant hydrogel comprising 5:7.5% w/v 700:8000 MW PEG-DA and 15% w/v alginate, to print the aortic wall and leaflets, respectively. An on-board UV-LED photocrosslinking module was also mounted directly below the syringe carriage to enable simultaneous 3D extrusion printing and in situ photocuring of the hydrogels. The shape fidelity of the printed aortic valves was evaluated using surface deviation analysis through micro-CT imaging and comparing with the native STL file. This analysis showed that shape fidelity of up to approximately 93% was achieved, although the shape fidelity decreased for smaller printed valves. Regardless, these results showed that the printing technique employed was capable of generating scaffolds with high geometric precision. Furthermore, printed scaffolds seeded with porcine aortic valve interstitial cells (PAVICs) maintained near 100% viability over 21 days, which highlights the potential of this 3D printing approach as a customizable tissue engineering-based solution for defective heart valve patients.

The summarized examples denoted above demonstrate some of the biologically-inspired applications that are enhanced through increasing the scope of multi-stimuli responsive materials and AM methods that utilize them. Applications, such as printed cell-laden aortic valves, were not conceivable without a method to manufacture them. With increased research into expanding the scope of multi-stimuli responsive materials and AM printing methods facilitated by these responses, a wide range of currently inconceivable applications may become available.

Additive Manufacturing to Produce Stimuli-Responsive Materials and Devices

In this section, we highlight breakthroughs in AM that demonstrate utilization of stimuli-responsive materials whose function is unleashed *post-printing*. In this regard, stimuli-responsive build materials can pose a caveat to AM in that the activation of the material is to be avoided during the manufacturing and processing of the final product. Once complete, the device is rendered functional due to the specific input-output nature of the responsive constituents. A major challenge for the incorporation of stimuli-responsive materials into mainstream production has commonly been the time-intensive, multi-step fabrication processes to make functional objects. AM has the potential to rapidly evolve the capabilities of the industrial manufacturing processes and access complex functional, even multi-material, devices in a single step. Incorporation of stimuli-responsive materials within AM further catalyzes this growth, producing forms and functions not possible otherwise.

Shape memory polymers

Shape memory polymers (SMPs), as briefly introduced previously, have different initial (permanent) and programmable temporary geometries. Programming of a desired temporary shape is achieved by energy input to kinetically lock the material into a higher energy conformation. Upon exposure to an external stimulus, the material can overcome kinetic barriers, thus enabling a return to the "remembered" initial shape.[68] The actuation that happens during this transition is called a shape memory effect (SME). Most SMPs are thermally-responsive polymers, however, a number of stimuli have been shown to elicit SMEs from many different materials. These phenomena are well-understood and have been thoroughly documented in various review articles previously.[68-72] The 3D printing of SMPs has drawn considerable interest, as the control of complex geometries

combined with an added dimension of responsiveness can yield extraordinary degrees of functionality. The most widely printed SMP is PLA, which is commercially available and one of the two most popular materials (the other being ABS) for melt material extrusion (MME).[73] Other SMPs that have been printed using MME include a PLA/hydroxyapatite composite and a commercially available polyurethane.[74, 75] Many other materials and printing methods have been reported as well, including several formulations of UV polymerizable inks and resins, block copolymer filaments, bioresins, and even powder bed fusion-printed shape memory alloys.[76-88] The development of these 3D printable SMPs has spurred intensive growth in the fields of 4D printing, leading to research into areas such as active origami, in which 2D sheets are controllably folded into complex 3D shapes, and smart actuation, in which SMPs are used to create functional moving objects such as grippers and valves.

SMPs are excellent candidates for active origami, a method that enables functional and dynamic three-dimensional modalities by using self-folding 2D materials. Dickey and co-workers showed that the self-folding of 2D polystyrene films could be achieved easily through differential heating induced by black ink, transforming their flat sheets into 3D structures.[89] Zolfagharian and co-workers expanded on this by making printed polystyrene actuators that also utilize the photothermal effect to enable controlled self-folding of their structures.[90] Zhang and co-workers evaluated the autonomous programming that occurs during the MME printing of PLA. They showed pattern transformation in lattice structures and self-folding sheets by MME of PLA, optionally using composite sheets with a different coefficient of thermal expansion.[91,92] As heat-shrinkable PLA is extruded from a nozzle, stress and strain are stored in the polymer as its relaxation is inhibited by its adhesion to either a build plate or previous PLA layers. As the polymer cools below its T_g this residual stress programs a temporary shape. Upon reheating, the polymer will assume its permanent shape as shown in Figure 5. Work by Dunn, Qi, and co-workers has significantly advanced the field by pioneering the use of multi-material photo-jetting to create functional folding materials.[93,94] By 3D printing SMP fibers within an elastomer matrix, they demonstrated that a flat printed object could be outfitted with directionally controlled folding hinges. They described a theoretical model with design parameters of fiber dimensions, hinge length, programming strains, and temperatures to enable control of complex motions. Applying this model, they constructed a self-folding origami box, pyramid, and airplane. In a separate report, they demonstrated the jetting of a SMP/elastomer bilayer that stores strain to autonomously program a SME during printing.[95] These works demonstrate the level of innovation possible for 3D printed SMP devices utilizing a single SMP material and clever design. For more complex devices, multi-responsive systems and advanced printing techniques are required.3D printed SMP composite materials with dual stimuli responses have been presented by several groups. In one report, Leng and co-workers extruded a SMP ink with iron oxide nanoparticles interspersed throughout such that their device exhibited a SME when exposed to either heat or alternating magnetic fields.[96] Chen and co-workers printed a photoresponsive polyurethane SMP composite by MME which uses photothermal activity of carbon black to activate the shape memory response, additionally showing potential for these materials downstream in printed electronics.[97,98] In another report, Rodriguez and co-workers used material extrusion to print a conductive thermo-setting SMP composite epoxy resin that was responsive to temperature and indirectly to resistive heating.[99] A unique feature of this material is that origami folds could be applied before fully thermosetting their resin, enabling their permanent shape to be 3D and their programmed (temporary) state to be a simple flat sheet or alternate 3D architecture.

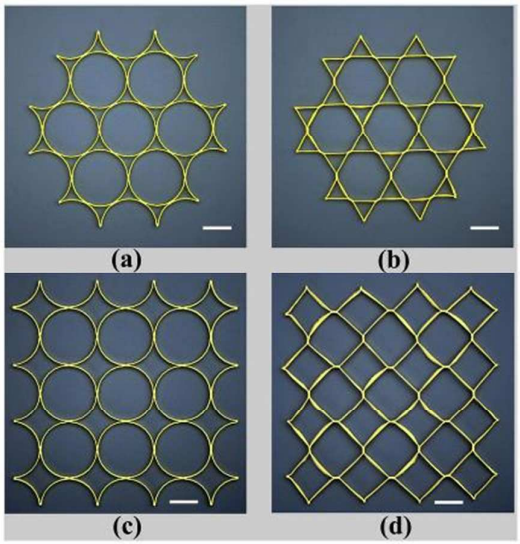

Figure 5. The 2D lattice materials, consisting of thin-walled PLA rings, are arranged initially in hexagonal pattern (a) or square pattern (c). The circular rings in the hexagonal or square lattices are transformed into hexagons (b) and quadrangles (d), respectively, when heated up to 90°C. Scale bar is 12 mm. Reprinted from ref. 91.

With the advent of 3D printable SMPs, the dimension of time can now be used to autonomously manipulate 3D printed objects. This process is often called 4D printing and it can be used to construct devices that can respond on demand to perform a range of functions. One of the first reports of 4D printed functional objects was by Raviv and co-workers, who photo-jetted encapsulated hydrogel joints that could later be swelled to induce macroscopic bending.[100] While not stimuli-responsive, this work has been expanded upon separately by various groups who have each used similar printing processes with SMPs to fabricate stimuli-responsive geometric changes. For example, Bettinger and co-workers embedded vascular structures into shape memory materials to enhance thermal diffusion and hence actuation rate.[101] Applications in biomedical engineering have also inspired innovations, such as the work of Senatov and co-workers who evaluated biocompatible 3D printed SMP scaffolds for potential use as self-fitting bone implants.[102] Liao and co-workers modelled and printed actuating SMP lattices and metamaterials, demonstrating potential biomedical and engineering

applications such as self-folding tubular stints, self-bending structures, self-tightening sutures, and self-coiling/deploying stents.[103-105] Adapting MME processes, both Chen and co-workers and Monzón and co-workers filamentized commercially available thermoplastic polyurethane elastomers (TPUs) with shape memory responses and fabricated functional devices such as a gripping device and extending coil.[106, 107] Using vat photopolymerization, several groups have demonstrated additive manufacturing of SMPs with detailed feature resolutions between 0.1 mm and 1 µm. Magdassi and co-workers used methacrylated poly(ε-caprolactone) (PCL) and a digital light processing setup to demonstrate how a SME could be used to control an electronic circuit.[76] This material was later applied to 4D print easily implantable trachial stents in a follow up demonstration by Cohn and co-workers.[108] Subsequently, Dunn and co-workers reported the use of micro-projection SLA to print an acrylate-based PEG network into impressively detailed SMP objects including functional gripper devices and "flowers" that appeared to bloom.[77] Additionally, Latanda and co-workers used laser SLA to print epoxy-SMP micro-vascular actuators, which used heated water within their internal vascular network to provide controlled actuation.[109] These printing techniques show control over actuation and the practical functionality of SMP devices. Most recently, others such as Yu and co-workers and Choong and co-workers have replicated the high resolution SMP printing of previous reports with new higher performance SMP materials..[110, 111] A particularly exciting demonstration of the power of 3D printed shape memory actuators was achieved by Choi and co-workers, who were able to construct a walking soft robot with a spider-like gait gained by actuation of a shape memory alloy stimulated by electrical signals.[112] The robot was constructed with a custom photo-jetting printer with rotatable print heads that automatically embedded shape memory alloy wires into a matrix of hard epoxy and flexible polyurethane material. By modulating the electrical signal each leg received, the robot was able to actuate and contract legs to create a walking motion, achieving an ultimate speed of 2.7 mm s^{-1}.

Even though 4D printing with a single SME can create functional devices, still more control over how structures move is desirable. Using multifunctional devices that have multiple responses to a stimuli gradient or unique responses to various stimuli can help achieve smart actuation. 3D printing is well-suited to enable such devices, as multi-material and gradient material printing capabilities can produce the complexity needed to access more degrees of control. Luo and co-workers have demonstrated 3D printed smart actuating devices using a MME printing process of customized styrene/methyl acrylate (St/MA) filaments.[113] The T_g of each polymer was tuned by synthesizing block copolymers of St-*b*-(MA-*co*-St)-*b*-St with different ratios of styrene to methyl acrylate in the center block. Multi-material MME was used to fabricate devices that showed control over the recovery sequence of their printed segments. This work was followed by Feng and co-workers who melt-blended commercially available polymers to form MME filament with quadruple SMEs.[114]

Several groups have produced examples of smart actuating devices using a photo-jetting process. Photo-jetting, while having a higher barrier to entry than other AM technologies, is particularly qualified to meet the complexity demands of smart actuating devices. Liu and co-workers printed multi-stage responsive SMP structures by controlling the geometric thickness of their print, as well as self-morphing structures using multiple SMP materials.[115,116] Dunn, Qi, and co-workers have demonstrated a variety of methods to control photo-jetted SMP devices. By varying the ratio of two SMP inks, they utilized seven different ink formulations with T_g's that ranged from 31 to 64 °C for the cured materials.[32] The different formulations enabled devices with sequential folding behaviour such as a self-locking box fabricated from a flat, 3D printed sheet of various SMPs. The temporally-controlled folding was used to correctly sequence folds to avoid collisions of segmented mobile parts and obviated the need for controlling thermal gradients within the device. In a subsequent report, they showed that two types of SMP fibers can be embedded into a 3D object with controlled geometries to create dynamic actuation profiles with changing temperature.[117] The addition of a second SME was utilized to produce a flat-bent-flat actuation scheme and a device was fabricated to either pick up or release an object in water at a certain temperature threshold. While the off-on-off scheme is a significant improvement to normal SMP actuation patterns, it still does not solve the problem of having to manually program temporary shapes to achieve a repeated actuation. However, in a new device paradigm Dunn, Qi and co-workers recently printed reversibly actuating devices comprised of an SMP, a swellable hydrogel, and a flexible matrix material. The swelling force of the hydrogel acted as the straining force necessary to program the temporary shape of the SMP.[118] When this force was removed by dehydration of the hydrogel, the SME guided recovery to the original shape. This actuation cycle was used to construct a reversible bench/ladder, actuating 2D lattices, and self-folding/unfolding flower.

These printing techniques highlight the practical functionality of SMP devices and the large potential for future improvements. To advance the field of 3D printed SMPs, improvements in design and modelling are needed to predict a priori the performance of SMP actuators and enable designers to fabricate devices with desired functionality. New custom materials should be developed to enable more complex and stronger actuations. Similarly, better methods of applying external stimuli such as photothermal, microwave, and joule heating, should be utilized to produce fast actuating structures necessary for real-world applications. Advances in large area printing should be pursued to allow for active origami structures with dramatic changes in size that are useful for deployable structures. Finally, new multi-material 3DP processes must be pioneered to allow for the combination of many types of stimuli responses in a single print. These techniques can be used to produce better SMP devices with reversible actuation schemes for repeated autonomous use, structures that are able to respond intelligently to their outside environment, and soft robots capable of locomotion.

Mechanochromic materials. Polymer mechanochemistry involves the transduction of macroscopic mechanical force into molecular levels of strain along a segment of a polymer backbone or network. This strain dictates geometric distortions in a mechanoresponsive moiety, or mechanophore, and modifies the potential energy surface to facilitate a chemical reaction. As a burgeoning field itself, there have been few examples of integration of mechanochemistry with other disciplines. Recently, Boydston and co-workers have demonstrated the MME printing of mechanochromic objects.[119] They investigated a 3D printable custom PCL filament that contained mechanochromic spiropyran units in each polymer chain. When printed test specimens were mechanically strained (e.g., through tensile elongation or torsion), the molecular-level response was a force-driven conversion of the spiropyran mechanophores into a highly colored merocyanine isomer. Notably, the custom filament required very little spiropyran to cause a visible color change upon activation. Specifically, filaments with as little as 0.25 wt % spiropyran (ca. 1 spiropyran unit each, in one-tenth of the polymer chains) was found to give intense color changes in most test specimens. In one demonstration of multimaterial printing, the authors used dual extrusion to fabricate a series of force sensors that contained multiple mechanochromic PCL regions throughout the gauge region of the specimen. These PCL regions could be activated in a predictable fashion, with sequential activation requiring increased peak mechanical load. This work demonstrated that 3D printing custom mechanochromic materials provides an easy way to fabricate prototypes with variable geometries and spatially-defined mechanochromic regions.

This initial report on integrated mechanochemistry and AM highlighted several parameters that may be key to realizing other mechanoresponsive AM build materials. For example, the authors did not observe activation of the spiropyran during extrusion, neither in the filamentation nor printing. Although this would not have been detrimental since the spiropyran activates reversibly, other mechanophores may activate under demanding extrusion conditions.[120] Additionally, the thermal stability of mechanophores must be considered when melt material extrusion is the targeted printing technique. For example, the authors specifically selected PCL for its low processing and printing temperatures. Finally, the high molar absorptivity of the merocyanine form (activated spiropyran) allowed for low (0.25 wt%) concentrations of mechanophore to be used. This caused essentially no changes in the physical properties of the PCL print material, which is an advantage that may not be enjoyed if higher concentrations of mechanophores are required. That is, printing with non-traditional polymer filaments is expected to require additional optimization.

Boydston and coworkers also incorporated a “flex-activated” mechanophore within vat photopolymerized materials.[121] In these novel mechanophore systems, straightening of polymer chains under mechanical load increases the bond angles within the mechanophore inducing a cycloreversion reaction, such as retro Diels-Alder reaction, and thereby release of a small molecule such as furan. Boydston and coworkers utilized this small molecule release as a reporter molecule to quantitatively assess and compare strain distributions between different complex geometries. Due to the thermal instability of the oxanobornadiene Diels-Alder adduct, AM and other manufacturing method that require heating would be unable to manufacture this material. Digital light processing (DLP) AM, a form of vat photopolymerization that uses a DLP projector to cure entire layers of material at once, was thereby used to print objects at room temperature. Different activation profiles were observed when compressing an octet truss versus a gyroid cube or 8D cubic lattice, suggesting the mechanophore could be used as molecular level strain probe for sensing the strain distribution differences generated by object geometry. Specifically, compression of printed octet truss unit cells, 8D cubic lattice, and gyroid lattice to 80% global strain increased the activation of the mechanophore to 3.1, 2.2, 2.5 times respectively compared to the uncompressed objects. The octet truss unit cells and gyroid lattice showed steep increase after 60% global compressive strain, whereas the 8D cubic lattice exhibited a linear activation profile, indicating clear differences in localized strain distribution within the different printed geometries. Downstream investigations may include designing mechanophores that can release small molecules and change colour at the same time upon activation, providing both quantitative and qualitative assessment of the strain distributions in complex geometries.

Photochromic and photoluminescent materials. Commercially, many photochromic filaments have recently become available. Photochromic molecules such as spiropyrans, spirooxazines, and diarylethenes are potential candidates for the dyes that make the filament photochromic. Spiropyran, one of the more academically studied photochromic molecules, is also capable of having a color changing isomerization upon radiation with ultraviolet (UV) light, as well as photo-relaxation with subsequent exposure to visible light or heat. Interestingly, the modular nature of the spiropyran moiety has enabled dually and selectively responsive systems involving photochromism and the previously described mechanochromism.[119] Printed specimens with segregated photochromic and mechanochromic regions were fabricated by alternating deposition of the two stimuli-responsive materials with a multi-material MME printer. AM provided an easily obtainable and highly customizable way to fabricate photo- and mechano- dual responsive materials that could be selectively activated by UV irradiation in the photochromic regions or mechanical load in the mechanochromic regions, as shown in Figure 6. This level of spatial control and rapid prototyping with multi-material compositions would be challenging without integration of the materials with AM technology.

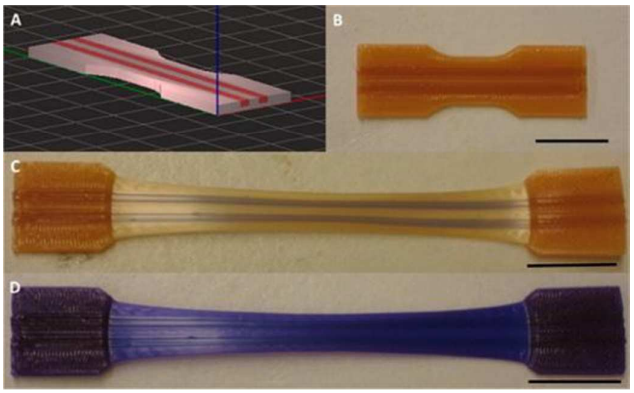

Figure 6. A) CAD representation of a multicomponent tensile test specimen, with red stripes indicating the location of the mechano-responsive filament (specimen body comprised of photochromic filament), (B) test specimen pre-elongation, (C) test specimen postelongation showing the mechanochromic response of the center lines, and (D) test specimen postelongation after 365 nm UV irradiation showing activation of both regions. Scale bars = 20 mm. Reprinted with permission ref. 119. Copyright (2014) American Chemical Society

Recently, photoluminescent 3D printed materials have also started to become more commercially available. Wang and co-workers have recently developed vat photopolymerizable photoluminescent resins.[122] Through dissolving photoluminescent dyes Rhodamine B, Solvent Yellow 98, and 2,5-*bis*(5-*tert*-butyl-benzoxazol-2-yl) (BBOT) into their diethylene glycol diacrylate-based resins, they were able to make red, green, and blue resins for SLA/DLP printing. Wang and co-workers optimized printing parameters for these photoluminescent resins through cure depth studies, and surprisingly found that the presence of Solvent Yellow 98 in their resins significantly decreased the cure depth of the resin, even more so than BBOT, which absorbs in the spectrum of wavelength emission and was expected to compete significantly with the polymerization. They attributed this drop to the naphthalimide subunit of Solvent Yellow 98, which has been demonstrated to be an efficient free radical scavenger, and so its interaction with the resin was more detrimental than BBOT's competition with the photoinitiator. Through these cure depth optimization studies, they successfully printed vases that photoluminesced under UV exposure using each of the dyes. These studies nicely demonstrate how photophysical responses (photoluminescent additives) can be combined with photochemically responsive materials (resins) to create exciting functional materials.

Kennedy and co-workers applied the fluorescent properties of lanthanide nanomaterials to melt material extrusion toward anti-counterfeiting applications.[123] They produced a novel PLA-based thermoplastic containing 11 wt % lanthanide-aspartic acid nanoscale coordination polymers (Ln^{3+}-Asp NCs). A solution casting procedure was used to disperse the Ln^{3+}-Asp particles into the PLA, after which a custom extruder was used to produce the filament. By varying the lanthanide of the nanoscale coordination polymer between terbium and europium, they could make green or red UV-photoluminescing PLA filaments. Using these filaments, they then printed raised structure QR codes on premade melt material extruded base squares. These QR codes could then be photographed when photoluminescing under UV light, and tracked back to the base QR code transaction, combining digital accountability in the form of blockchain technology with physical anti-counterfeiting.

The interconnection between AM and medical fields has led to research into printing materials that mimic the behavior and physical properties of tissues and organs. Generating 3D printable tissue-like materials requires a constant advancement of not only the materials used, but also their stimuli response. Recently, Bayley and co-workers have made tissue-like materials consisting of synthetic cells printed using a water-in-oil droplet 3D printer.[124] In an extension of this work, Booth and co-workers were able to incorporate a photoswitchable red fluorescent protein into their printed tissues.[125] Upon exposure to blue light, the protein fluorescence turned to the ON state, and exposure to yellow light turned the protein to the OFF state. This reversible fluorescence was repeated for over 15 cycles. Using this protein, they used light to pattern and then reset fluorescence within their printed tissues, forming droplet shapes like an "X" and an "O", each visible through a confocal fluorescence microscope. These materials are exciting candidates for applications that combine synthetic and living tissues. One potential application for these reversible and stimuli-responsive synthetic tissues could be used to interact or stimulate the activities of target cells and tissues within the body, such as targeting specific neuronal pathways.

Optomechanically responsive materials. Irradiation with broadband visible light can induce mechanical changes in 3D printed materials. For example, Shear and co-workers utilized microscopic dynamic mask-based 3D printing to fabricate protein-based hydrogels that underwent photoexpansion or photocontraction due to the interactions between light and the charges on photosensitizers and protein-based hydrogels.[126] Unlike traditional synthetic polymers that are often inert to phototriggers used for biological applications, these protein-based hydrogels are highly functionalized and tunable for culturing and safely encapsulating cells in response to light. 3D printing these synthetic materials resulted in complex structures that could be used as microchambers capable of manipulating cells remotely. The photoexpansion and photocontraction gates of these microchambers were made of two different photosensitizer/protein-based hydrogel combinations (Figure 7).

One system used negatively charged Rose Bengal/Bovine serum albumin (RB/BSA). This RB/BSA combination could expand under green light and was used to create open pores that switched to a closed state after photoactivation. Positively charged methylene blue/lysozyme (MB/Lys) based printed materials, with the properties of photocontraction, were made as closed pores that opened upon photoactivation with red light. The controlled opening and closure of these gates facilitated cell motion within multiple hierarchical chambers in these microenvironments. The RB/BSA reagents were both negatively charged, while the MB/Lys were both positively

charged, raising challenges in the ability to 3D print these two combinations of materials together. To print a combination of these materials, the first printed charged material had to be soaked into a reagent solution of the second material. If the second material was oppositely charged, this resulted in a decrease in the degree of photoresponsiveness of the final object due to charge perturbation. The researchers overcame this issue by printing the negatively charged RB/BSA material first, then incorporating the positively charged MB/Lys material, followed by rinsing the final printed structure with a low concentration of RB to restore the negative charge and photoexpansion capability of the RB/BSA material without influencing the photocontraction capacity of the secondary MB/Lys material.

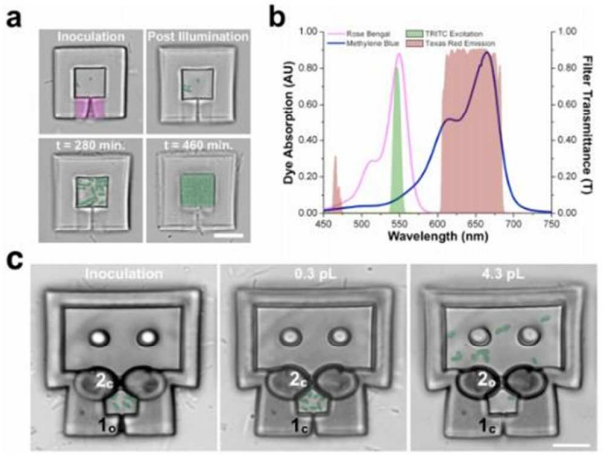

Figure 7. Functional cell enclosures. The light-responsive properties of protein hydrogels can be used to corral and release bacterial populations within picoliter volumes. (a) P. aeruginosa cells swim through an open aperture in a RB/BSA structure (top left), and are then trapped by swelling the aperture closed with a 15 min exposure to light (top right). Bacteria divide at a normal rate to fill the cavity over ~8 h (bottom panels). The pink region in the top left panel shows the region of lower-density hydrogel. (b) RB and MB absorption spectra, and transmittance spectra of TRITC excitation and Texas Red emission filters, demonstrate the ability to excite these photosensitizers using distinct spectral components with only minor cross-talk. (c) A hybrid bacterial edifice composed of an RB/BSA pore (lower portion of image) and a MB/Lys pore (paired ovals) demonstrates the ability to sequentially close and open chambers to capture, grow, then dilute P. aeruginosa. Bacteria swim into a small antechamber through pore 1 (1_o) in its open state, and are allowed to accumulate for a short period (left panel). Illumination of the edifice through a TRITC excitation filter causes swelling and transition of pore 1 to a closed state (1c) while the MB/lys aperture, pore 2, remains in a closed state (2c), thereby restricting cells to a 0.3 pL chamber (middle panel). Following division over a period of 1 h, cells are released into a 4.3 pL chamber by illuminating the sample through a Texas Red emission filter to open the MB/Lys pore (2o; right panel). Bacteria in all images are false-colored green for visualization. Scale bars, 10 µm Reprinted with permission from ref. 126. Copyright (2016) American Chemical Society.

Electroluminescent materials. Quantum dot light emitting diodes (QD-LEDs) with electroluminescence properties can emit light upon applied voltage. Unfortunately, current manufacturing costs are still too high to produce objects with quantum dots on a large-scale. AM, with its ability to rapidly modify and change outputted structural designs, could be an attractive process toward reducing the costs of production of objects containing quantum dots. In addition, the incorporation of quantum dots into 3D printed objects could also give rise to 3D objects with unique optical properties, which could be beneficial toward applications such as anti-counterfeiting.[127] McAlpine and co-workers used melt material extrusion to fabricate and assemble layers of QD-LEDs, achieving fully 3D printed active multi-material electronic devices with diverse functions.[128] The electroluminescence effects of these devices were finely tuned by varying the dispersion of QDs and the thickness of semiconducting layers. By combining the 3D scanning of topological surfaces and MME, QD-LEDs could be fabricated on flexible curved surfaces, offering a new way to manufacture seamless interwoven electronic devices. This conformal printing technique scanned the geometry of a curved surface and merged the QD-LED component with scanned data in software to print the devices. This successful result shows the versatility of 3D printing and could be advantageous toward fabricating wearable devices and flexible displays on non-flat surfaces.

Photoconductive transcription. Using the water-in-oil droplet 3D printing approach developed by Bayley and co-workers,[124] Booth, Bayley and co-workers incorporated a DNA promoter within printed cells that responded to light.[129] In this way, they have been able to turn on the activation of specific genes through the use of this light-activated transcription promoter. They demonstrated this by placing a gene that controlled cell membrane porosity downstream from the transcription promoter. In the presence of light, the porosity of the cells that contained the DNA promoter was increased, enabling an increase in transfer of compounds such as dyes and ions for electrical signalling between cells. This thereby increased conductivity. With multi-material control over which cells contained the DNA, as well as control over which cells were illuminated via a photomask, they showed it was possible to direct where the stimuli response was present. In this way, they were able to fabricate functional neuronal transmission mimics in a controlled fashion. Further work by Booth and co-workers showed that by varying the amount of time of UV irradiation, they could vary the level of photoluminescent protein expression within their droplets.[125] Downstream use of these materials could include incorporation into soft biodevices that are integrated with cellular tissue.

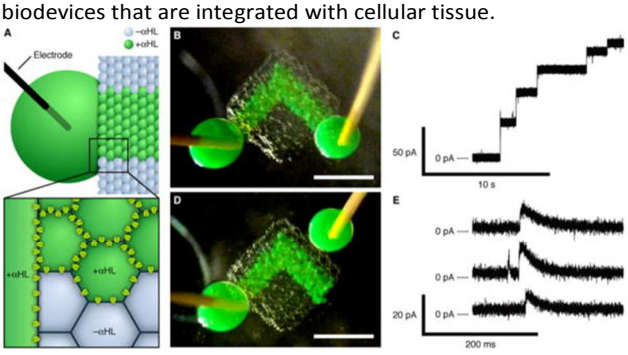

Figure 8. Electrically conductive pathway. (**A**) Schematic of part of a network printed with an ionically conductive pathway. Only the green

droplets and the large drop contain αHL pores. The large drop is impaled with an Ag/AgCl electrode. The magnified section illustrates the αHL pores in the bilayers around the αHL-containing droplets. (**B**) Photograph of a printed network with electrode-impaled drops placed on either end of the conductive pathway. The green droplets contain αHL, while the other droplets contain no protein. Scale bar, 500 µm. (**C**) Stepwise increase in the ionic current as measured in the configuration in (B), at 50 mV in 1 M KCl at pH 8.0. (**D**) Photograph of the network in (B), after separating one of the large drops and rejoining it onto the network away from the conductive pathway. Scale bar, 500 µm. (**E**) Selected portions of a single recording as measured in the configuration in (D) at 50 mV, showing transient increases in ionic current. From ref. 124. Reprinted with permission from AAAS.

Photothermally active materials. The photothermal effect is a phenomenon whereby heat is generated from the photoexcitation of materials. Photothermal differential heating between light and dark materials has been used as one of the ways to enable SMP actuation. [89,90,97,98] For example, Nelson and co-workers reported a method to incorporate of MWCNTs into their hydrogels to afford photothermally active composite objects capable of actuation when irradiated with a near-infrared laser.[61] In another example, McAlpine and co-workers investigated using the photothermal effect in ME hydrogel capsules as a means for drug delivery.[130] The core of the capsules was comprised of nanoparticles with a biomolecular payload, and the shell was comprised of hydrogels functionalized with gold nanorods (AuNRs) (Figure 9). The AuNRs absorbed infrared light in the localized surface plasmon resonance (LSPR) wavelength ultimately leading to heat generation. The thermal energy caused the rupture of the capsules when illuminated, leading to the selective release of functional biomolecules. In this case, AM enabled the researchers to control the spatiotemporal distribution of the functional particles and create highly complex structures. For example, 3D arrays of capsules were directly printed in transparent hydrogel matrices with cylindrical or cubic shapes to form hierarchical structures. These differences in shapes and hierarchical structures could be used in future applications to control the kinetic profile of payload delivery.

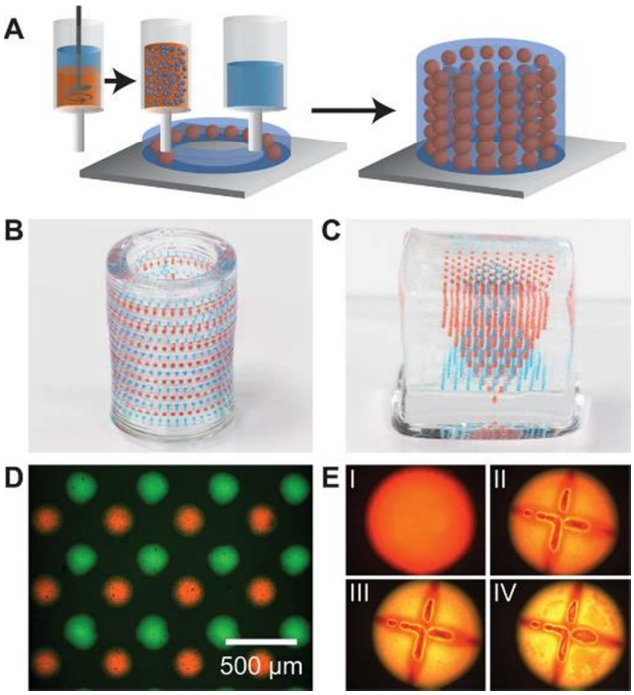

Figure 9. 3D printing of hierarchically multiplexed capsule arrays. (A) Schematic illustrating an emulsion ink-based method to 3D print complex capsule arrays. The emulsion ink is prepared by directly dispersing the aqueous core in the PLGA solution. The hydrogel and emulsion inks are sequentially printed in a layer-by-layer manner to form a 3D structure. (B, C) Optical images of 3D multiplexed capsule arrays directly printed in cylindrical and square hydrogel matrices, respectively (colors of the capsules are from food dyes in the dispersed cores). (D) Fluorescent optical image of a single layer of a multiplexed emulsion-based capsule array. (E) Fluorescent optical images showing rupture and release of fluorescein dye (poly(fluorescein isothiocyanate allylamine hydrochloride)) from an emulsion capsule with Nile red stained PLGA (I: before laser rupture; II, III, IV: 15 min, 1 h, and 2 h after laser rupture; diameter of the capsule: ~300 µm). Reprinted with permission from ref. 130. Copyright (2015) American Chemical Society.

Piezoelectric and piezoresistive materials. Advancements in the additive manufacturing of electronics have led to a number of functional conductive devices,[131-142] which includes a number of piezoelectric and piezoresistive materials. Piezoelectrics transform mechanical stimuli into electrical charge or voltage, whereas piezoresistive materials increase in resistance. A converse piezoelectric effect is also capable of stretching or compressing a material in response to an ambient electrical field. 3D printing can facilitate the fabrication of 3D-structured piezoelectric polymer composites. Kim and co-workers developed piezoelectric materials by crosslinking acrylate-functionalized barium titanate (BTO) nanoparticles within a polyethylene glycol diacrylate (PEGDA) matrix via digital projection vat photopolymerization.[143] The mechanical-to-electrical conversion efficiency of materials containing the crosslinker modified nanoparticles was ten times greater than that of the material with unmodified nanoparticles. This opens up the potential to use these materials toward applications that involve highly-ordered 3D piezoelectric devices utilized in acoustic production, energy harvesting, and microbalancing.

Another example of the use of additive manufacturing to create piezoelectric devices comes from the work of Woodward and co-workers.[144] By incorporating piezoelectric ceramic components into an acrylate based microstereolithographic resin, Woodward and co-workers printed the green bodies of their structures with complex geometries. These green bodies were then gradually heated to 600 °C, and then kept at that temperature for one hour to pyrolyze all of the organic components in their objects. Shrinkage was visible in the structures after sintering, with a shrinkage of 25.4% occurring perpendicular to the layers and a shrinkage of 24.0% in line with the layers. This difference in shrinkage is due to the inherent anisotropy of layer-by-layer printing methods. The piezoelectric performance of samples made through this method were comparable to those made by other more conventional methods, though the remnant polarization of the printed compounds was slightly lower, and the coercive field slightly higher, likely due to the increased porosity of objects. Ceramics prepared in this method had an anisotropic piezoelectric modulus, or d_{33}, based on the direction of testing. The piezoelectric modulus, a measure of the volume change when an electric field is applied, was lower in the direction perpendicular to the printed layers. This effect could be useful in piezoelectric arrays by decreasing the cross-coupling between array elements.

Leigh and co-workers reported the MME of a conductive, piezoresistive composite termed carbomorph.[145] Using polycaprolactone as the base polymer, they added in 15 wt % of carbon black as a conductive filler and then filamentized the material. They used this composite filament to print strain sensors and human-interface-devices (HIDs) that could measure the change in resistance in response to flexing of the material. Adding more carbon black to the polymer would increase the conductivity of the material, and generally 25% of a filler is needed to turn an insulating material into non-insulating. Unfortunately, an inherent limitation to this printing system was that adding more than 15% of the carbon black to the PCL made the material unable to pass through the nozzle of the filament printer. Nevertheless, the demonstration showcases some of the potential in this area.

Kim and co-workers used melt material extrusion process to fabricate multiaxial force sensors using thermoplastic polyurethane filament containing carbon nanotubes (CNT/TPU).[146] Using a shear melting process to disperse the nanotubes into the thermoplastic polyurethane, they achieved good dispersion of the nanoparticles without agglomeration. Using a dual head extruder, they printed multiaxial force sensors with a minimal amount of CNT/TPU sensing regions. Force applied in x, y, and z directions could be detected repeatably with the sensor. This could be useful for potential downstream applications such as real-time patient movement monitoring during rehabilitation processes. The use of a polyurethane elastomer-based filament enabled a wider deformation range than possible with other thermoplastics like PCL. Some dynamic response was lost, however, because of the viscoelasticity of the material, and some hysteresis was present in repeated cycling.

With a newly developed technique, referred to as embedded 3DP, Lewis and co-workers fabricated a stretchable electronic strain sensor.[147] Their embedded 3DP technique uses ink or fluid that is deposited and encapsulated within a vat of viscous, elastomeric matrix resin. The matrix resin is then cured using UV light, producing a monolithic part. Lewis and co-workers embedded conductive carbon grease, which contains particles of carbon black suspended in silicone oil, within an elastomeric matrix. The resulting printed object was a highly stretchable piezoresistive device in which the resistance of the conductive ink layer was increased when stretched. By modifying print speeds, it was found that sensors printed at a higher speed showed a smaller cross-sectional area, and that these sensors displayed a greater overall change in resistance. Samples printed at 4 mm/s had an initial resistance of 60 ± 3 kΩ and an overall change in resistance of 300 kΩ at 100% tensile strain. Samples printed at 1 mm/s, resulting in a larger cross-sectional area, had an initial resistance of 11 ± 2 kΩ and overall change in resistance of 50 kΩ at 100% strain. While the change in resistance can be tuned in this matter, it is limited by the loss in print definition that comes with samples printed at slower speeds. The authors also noted the presence of hysteresis in their electrical performance under cycling. This hysteresis is caused by the differences in time-scales between stretching of the object and flow of the embedded ink, resulting in disruption of the polymer network at high strains. Following the breakthrough of stretchable printed electronics, one might envision further fine-tuning of the materials and process to achieve optimized devices suitable for long-term use.

Recently, Lewis and co-workers expanded and applied their embedded 3DP toward microphysiological systems, also known as organs-on-chips.[148] Using a different carbon black based piezoresistive ink, the group was able to create a cardiac microphysiological device with constant electric readout of the contraction of the cardiac tissue (Figure 10). Contraction of the physio-mimetic laminar cardiac tissue, attached to the printed cantilever, resulted in deflection of the cantilever and an overall stretch in the conductive gauge wire. This stretching was then electronically detectable by the change in resistance in a non-destructive and non-invasive fashion. This system enabled them to look at the effect of the delivery of different drugs into the cardiac system over the course of four weeks and measure the different responses of the cardiac tissue through the printed piezoresistive strain sensor. This research opens up new avenues to explore *in vitro* research in areas such as tissue engineering, drug screening, and toxicology. Lewis and co-workers have further used this embedded 3DP technique in combination with surface mounting of electronic components to produce a hybrid method of printing to create soft electronics.[149]

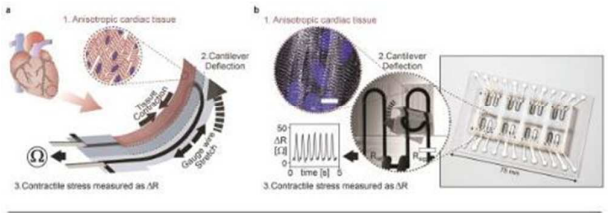

Figure 10. (a) Principle sketch of the device. Contraction of an anisotropic engineered cardiac tissue (1) deflects a cantilever substrate (2), thereby stretching a soft strain gauge embedded in the cantilever. This generates a resistance change proportional to the contractile stress of the tissue (3). (b) The fully printed final device. Insert 1: Confocal microscopy image of immuno-stained laminar NRVM cardiac tissue on the cantilever surface. Blue: DAPI nuclei stain, White: α-actinin, scale bar 10 µm. Insert 2: Still images of a cantilever deflecting upon tissue contraction. Insert 3: Example resistance signal. Reprinted by permission from Springer Nature: ref. 148.

In a separate approach, Kramer and co-workers designed a novel material extrusion printer to produce all-printed stretchable electronics.[150] An elastomeric matrix was extrusion printed as base for the device and patterned conductive layers of a liquid metal slurry were then sprayed onto the elastomer base before being mechanically sintered at room temperature to create conductive paths via automated tapping. Finally, another elastomer layer was extrusion printed around the conductive liquid metal to encapsulate and seal the device. The liquid metal slurry contained densely packed microparticles of Gallium-indium alloy (eGaIn), which forms a thin oxide layer in the presence of oxygen. This oxide layer is electrically insulating. Without activation of the deposited liquid metal with tapping, inducing rupture of the shell between the particles, the sprayed particles would not produce a conductive path. This printing method resulted in stretchable, flexible electronic devices, including piezoresistive pressure and strain sensors. Printing these devices on muslin fabric showed the future potential of these materials toward wearable electronics. The maximum elongation of the elastomeric device was greater than that of the fabric, indicating that the device would not limit the range of motion of the end user. One limitation to this novel printing method is the long cure time of the elastomer materials, 6 h at room temperature, or 2 h with a 60 °C heating bed.

In another example of AM of piezoresistive strain sensors, Kim and co-workers ME a piezoresistive composite material to create functional devices.[151] Using a polystyrene-polyisoprene-polystyrene (SIS) linear polymer base, they incorporated amine-functionalized multi-walled carbon nanotubes and 2D graphene oxide nanoparticles. The amine functionalization enabled the carbon nanotubes to be confined to the surfaces of the graphene oxides via anchoring onto negatively charged surface groups. The composite pastes they made through mixing various ratios of nanotube functionalized SIS 1,3-dichlorobenzene as a solvent. The pastes could maintain shape when stacked during 3D printing and were used to make strain sensing devices. These strain sensors were able to detect strains from 0-1%, as well as larger strains up to 50%, showing little hysteresis and a high gauge factor. For use in devices, it was necessary to extrude the pseudo-solid dough onto various substrates such as high porosity paper, nylon, poly(vinylidene fluoride), and polytetrafluoroethylene.

Functional tactile sensors have also been achieved via AM of piezoelectric materials. For example, McAlpine and co-workers utilized a multimaterial extrusion process [152] with silver-based nanocomposite elastomer inks as piezoresistive components and working electrodes. A combination of silicone elastomer and removable Pluronic^{TM} support layers were also extruded in a controlled fashion using four parallel nozzle heads. In this way, McAlpine and co-workers fabricated the complete sensor, consisting of four different types of material, in a continuous printing process. When testing the piezoresistive behaviour of these devices, the resistance of the device was found to decrease 12-fold under increasing pressures from 100 to 500 kPa. The devices showed negligible hysteresis and consistent responses for over one hundred cycles. Impressively, a device printed in this way was attached above the radial artery of an end user and used to monitor the physical force of a pulse in real time. The tactile sensor was worn for three consecutive days, and the sensing behavior remained unchanged. Additionally, McAlpine and co-workers used reverse engineering of a hand model to print devices directly onto a fingertip.

Materials with molecular recognition. The ability to print objects that include a level of molecular recognition could facilitate any number of interesting applications such as 3D printed bioassays, gas sensors, and wearable biological monitors. By extruding graphene oxide using a controllable liquid meniscus, Kim and co-workers extruded free-standing 3D reduced graphene oxide nanowires.[153] These nanowires were conductive, able to withstand strains upwards of 340% with little variation in electrical resistance, and maintained conductivity when stretched to 150% strain for over 120 cycles. The resistance of reduced graphene oxide is generally dominated by the presence of dominantly charged carrier holes. Kim and co-workers took advantage of this to make a transducer gas sensor for CO_2 using the nanowires within printed devices. The CO_2 being adsorbed into the nanowires resulted in a decrease of holes and thereby a decrease in resistance of the conductive material. They correlated the concentration of CO_2 to the degree of change in resistance of the reduced graphene oxide nanowires.

Chemiluminescence is another example of chemically induced stimuli response that has been integrated with AM. Using DLP AM vat photopolymerization, Marquette and co-workers incorporated chemiluminescent enzymes within printed hydrogel and acrylate plastic networks.[154] The enzymes responded to glucose and luminol, and in the presence of both emitted light. Using multiple vats of different resins, they controlled where the luminescence occurred based on the presence, or lack of, these compounds and enzymes within the printed multi-materials. They were also able to print interesting geometries that exemplified the ability to control response and chemiluminescence (Figure 11). For example, they printed propellers that could rotate freely on their axis and showed that in a solution containing the necessary

chemical triggers, they could increase luminescence on the propellers with increased rotation speed, as faster rotation resulted in higher mixing and more contact between the enzymes and the chemical triggers in solution. In a continuation of this work, Marquette and co-workers also printed in complex fanciful ball geometries using the same chemiluminescent enzymes, even showing the ability to separate the enzymes into different halves of the ball, localizing the luminescence to only one half of the ball.[155] Additionally, Marquette and co-workers incorporated an alkaline phosphatase enzyme into their vat photopolymerized hydrogel geometries, enabling in-situ calcification of their PEG hydrogels in the presence of calcium chloride and α-D-glucose-1-phosphate.[155]

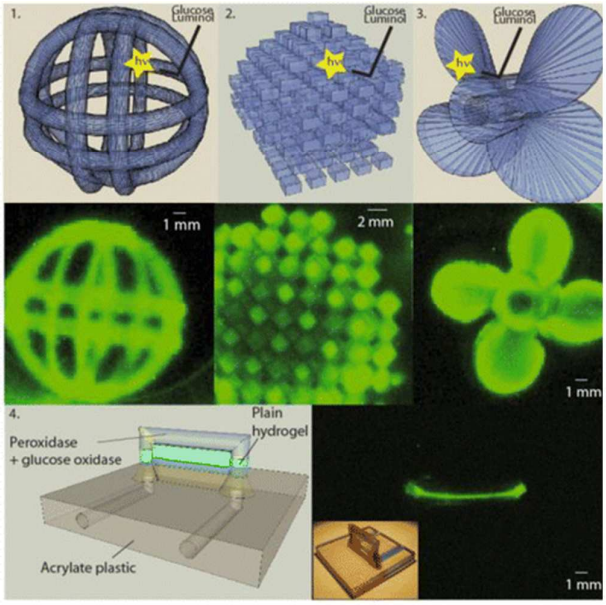

Figure 11. CAD design of four complex 3D hydrogel objects entrapping both horseradish peroxidase and glucose oxidase: (1) fanciful ball, (2) 3D pixel, (3) propeller, and (4) fluidic multicomponent object. Chemiluminescent images (3 min integration) were obtained in the presence of glucose 100 mM, luminol 220 mM, Veronal buffer 30 mM, KCl 30 mM, pH 8.5. Reprinted with permission from ref. 154. Copyright (2016) American Chemical Society.

Using methacrylated alginate (AA-MA), Ionov and co-workers fabricated 4D shape morphing hydrogel tubes using ME.[156] After extruding and photocrosslinking the AA-MA, the printed films of polymer would swell and self-fold into the shape of a tube. In the presence of calcium ions, the alginate would bind to the calcium, creating ionic crosslinks, causing the polymer to deswell and lose its folded shape. Using ethylenediaminetetraacetic acid (EDTA), the calcium ions could be removed from the polymer, enabling the films to swell again and return to their tubular swollen state. By varying the print parameters and percent methacrylate of their hydrogel inks, Ionov and co-workers were able to vary the shell thickness and inner diameter of the self-folding tubes. In this way they were able to achieve diameters as small as 20 μm, comparable in size to the smallest blood vessels, such as capillaries. In addition to their shape morphing response to calcium, the AA-MA gels were also biocompatible with cell viability maintained for 7 days.

Zhao and co-workers used living cells as responsive units in photocrosslinked ME printed logic gates and wearable sensors.[157] They use hydrogels containing multiple programmed bacterial cells. Specifically, they microextruded complex self-supporting geometries such as a cuboid, a pyramid, and a dome. Additionally, by printing multiple chemicals and chemical sensing programmed cells, they were able to replicate logic gates in which the cells responded to the presence or lack of one or more chemical inputs, such as Rham, aTc AHL, and IPTG. This resulted in a controlled and measurable response, production, or disappearance, of green fluorescent protein and thereby triggered changes in photoluminescence. In addition to creating Boolean logic gates, they measured the living characteristic of these responsive materials by visually tracking the spatial distribution of fluorescence over time. Visualizing this spatiotemporal responsive patterning could help program living material responses to chemical diffusion in the future. Finally, Zhao and co-workers printed a biosensing tattoo, in which three different programmed cell bioinks were used to print three discrete regions: one that responded to Rham, one to AHL, and one to IPTG. In the presence of any of these chemical inducers on the skin, fluorescence was produced in the correct portion of the tattoo, showing the potential for these printed living devices for wearable biosensors.

Other promising areas of chemical recognition, while not stimuli-responsive, have begun to be integrated with AM. For example, Baker and co-workers used DLP AM vat photopolymerization to encapsulate monooxygenase enzymes into a hydrogel matrix to enable methane to methanol conversion within a 3D printed object.[158] The enzymes retained 100% activity in the objects, without the energy and metabolic upkeep that would be required for a whole-cell based process. This could facilitate use of these 3D printing structures toward industrial methane-to-methanol conversion processes downstream, as well as future exploration into other gas-liquid biocatalysis reactions.

Thermo-responsive materials. 4D printing of hydrogels is an exciting area of study toward the development of smart materials.[159-162] Temperature-sensitive hydrogels are particularly interesting as they undergo a reversible volume transition through a coil-to-globule transition of the network strands, enabling actuation. Many researchers have used this thermal-sensitivity to enable or enhance the ability to 3D print these materials, as discussed in the first half of this review. Work has also been done to 3D print these smart materials where a thermally-sensitive shape change, distinct from a shape memory effect, is generated in the final 3D printed object. For example, Spinks and co-workers showed they could achieve actuation in printed alginate/ poly(N-isopropylacrylamide) (PNiPAAm) ionic covalent entanglement (ICE) gels.[163] PNiPAAm acted as both the thermally-sensitive trigger for actuation and the toughening agent making these gels mechanically robust. The gels were printed using a 3D-

Bioplotter system coupled with UV curing, and monomer inks with a constant amount of alginate, covalent crosslinker, and UV initiator, as well as varying concentrations of NiPAAm monomer. After printing and UV curing, the team used the lower critical solution temperature (LCST) of PNiPAAm (≈32-35 °C) to make valves that are open below the LCST (20 °C), but close upon heating past that critical temperature (experimentally demonstrated at 60 °C). After their initial work, Spinks and co-workers further went on to show how functional hydrogel devices could be made through multi-material 3D printing of multiple inks to form tough composite gels, as well as hydrogel objects with thermosensitive hinges and artificial muscles.[164-166]

Following this initial nozzle-based 3D printing work, Lee and co-workers also made alginate/PNiPAAm ICE based thermally-sensitive structures using projection based micro-sterelithography.[167] With layer resolutions as small as 40 µm, they used differences in layer thickness, light intensity, and crosslinker concentrations to modify the anisotropic swelling of the resulting printed objects. By varying alginate and ionic monomer concentrations they were also able to modify the critical temperature and the elastic modulus of the gels, respectively. More research on these materials may show them to be useful toward load bearing applications.

Thermo-responsive 4D printing can also be accessed using liquid crystal elastomers (LCEs). Ware and co-workers used the shear of material extrusion printing with an LCE-containing ink to align the liquid crystals into an ordered nematic phase along the print path.[168] This oriented ink can then be polymerized and locked into place with UV light. Heating the resulting printed structure transitions the liquid crystals from a nematic phase to a randomly oriented isotropic phase, triggering a reversible contraction around 40% in a simple uniaxial actuator. In a striking contrast to SMPs, this mode of shape change offers many unique and complex responses as the printing path dictates how a device actuates.

Liang and co-workers made crosslinked hydrogel bilayers that actuate under both heat and near-infrared light through ME.[169] The hydrogel inks used in ME were comprised mainly of NiPAAm, with nanofibrillated cellulose added to increase crosslink density and decrease hydrogel mobility, graphene oxide added to enable photothermal heating, and nanoclay added to increase actuation.[170,171] The hydrogel inks, containing a peroxide radical initiator and amine catalyst, were first extruded onto a glass slide, and then placed under a vacuum atmosphere at 25 °C for 24 h, enabling in situ free radical polymerization of the printed objects. Upon heating, or photothermal heating from a near-infrared laser, the swollen printed objects underwent actuation. The incorporation of AM with these actuating hydrogels enabled more intelligent actuator design, in which Liang and co-workers controlled how the printed discs folded.

Self-healing materials. Self-healing and self-reinforcing polymers are widely sought for their ability to return or improve upon their initial material properties in response to stimuli such as mechanical deformation, fracture, and heat.[172,36] Self-healing capabilities are motivated by the promise of enhanced lifetimes and endured strength even under multiple mechanical loads. Based on initial work in material extrusion and assembly of vascular networks done by Lewis and co-workers, Lewis, Sottos and co-workers reported 3D printing of self-healing materials.[173, 174] They created 3D vascularized structures containing dicyclopentadiene monomer within an epoxy matrix containing solid particles of Grubbs 1st-generation catalysts. Upon cracking of the epoxy matrix, the monomer from the vascular networks filled the void spaces made within the damaged material. Once in contact with the entrapped catalyst, the monomer was polymerized to heal the crack. [174] Continuing with this concept of vascularized networks, Lewis, Sottos and co-workers further made a self-healing material with vascular networks containing separate components of a two-component epoxy resin.[175] Upon propagation of a crack within the material, the two components would wick into the crack and come into contact, resulting in polymerization of the epoxy and healing of the material. While healing efficiencies of over 60% in 16 cycles were achieved, a major limitation determined through this system was that diffusion alone was not sufficient for effective healing in the two-part vascular system. Lewis, Sottos, and co-workers then moved to an active mixing approach.[176] Samples were initially loaded into a four-point bend geometry, and then put under load until a crack had formed at a specified scored point in the substrate, and material from the vascular networks had filled the space due to capillary forces. After crack formation, the matrix was loaded into cyclic flexural testing for 50 cycles, enhancing the mixing of the two components in the crack plane. Then, the material was heated at 30 °C for 48 h, resulting in curing in the areas where the epoxy resin had mixed. This same process of crack formation and cyclic flexural testing was then conducted again, controlling the cracking to be at the same specified location. The process was repeated for 30 cycles for each specimen, and a total of eight specimens. Through this process, they showed that the material maintained healing capabilities for over 30 cycles at the same location, retaining a healing efficiency of roughly 50% after the 30th cycle. While this system mitigated the slow rate of diffusion, the need for slow active mixing, and slow ambient curing of the self-healing materials with the crack plane may need to be addressed depending upon desired applications. Active pumping of healing agent to the crack plane may extend the healing cycles.[176] Further work by Lewis and co-workers helped mitigate these limitations by adding a third, thermal regulating vascular network into the material (Figure 12).[177] With this approach, a heated liquid could provide localized heating, enabling faster curing of the epoxy and amine hardeners within the damage site.

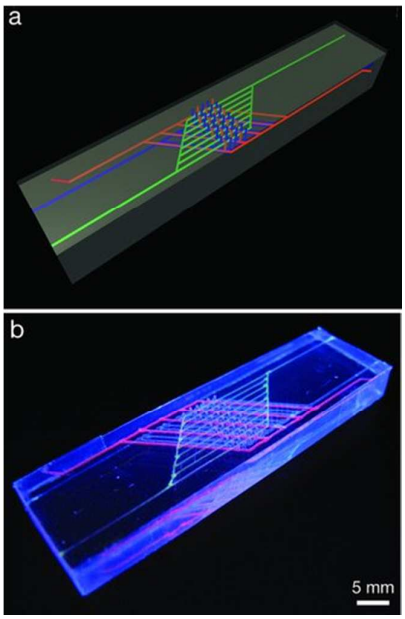

Figure 12. (a) Schematic view of epoxy coating/substrate architecture with embedded interpenetrating microvascular networks. Two of these networks house epoxy resin (blue) and hardener (red), while the third network provides thermal control (green) to accelerate healing kinetics after damage occurs. (b) Corresponding optical image of this novel self-healing system fabricated by direct-write assembly and then imaged with different fluorescent dye solutions within each network. Reprinted with permission ref. 177. Copyright (2011) John Wiley and Sons.

Li and co-workers used double-network (DN) hydrogels containing both ionic and covalent crosslinks to achieve material extrusion of self-healing strain sensors.[178] They synthesized a physically and thermally reversible double-network based on the polysaccharide *K*-carrageenan and polyacrylamide (PAAm) and characterized its self-healing behaviour. Through material extrusion of a heated pregel solution, followed by UV irradiation for 1 h, complex geometries such as a hollow triangular prism, a hollow cube, and tensile dogbone samples were printed. Storing cut printed tensile samples in polyethylene bags in a 90 °C water bath for 20 min resulted in healing and 92% recovery of elastic modulus and 85% recovery in energy dissipation. The *K*-carrageenan/PAAm DN hydrogels showed good electrical conductivity, and so resistance tests were also conducted that showed increase in resistivity with strain. A strain sensor was made by encapsulating the hydrogel in acrylic tape to prevent evaporation of water from the hydrogel and was used to monitor human motion in real time.

Xing and co-workers also used a DN hydrogel approach to achieve self-healing and piezoresistive material extrusion-based printed materials.[179] They did so using polypyrrole (PPy) grafted to a double-bond decorated chitosan (DCh) with pendant methacrylate groups, forming a DCh-PPy base gel. This DCh-PPy base gel was then chemically polymerized with poly(acrylic acid) (PAA) in the presence of ferric ions. When the hydrogel was cut into two halves and the pieces brought back into contact, self-healing occurred immediately under ambient conditions. After 30 s, 90% electrical recovery of conductivity was observed, and complete mechanical recovery was visible after 2 min., They ascribed the fast recovery time to dynamic interactions between PAA and PPy functional groups at the cut area, enabling migration of ferric ions between the two sides. Through applying compression to their printed objects, both the conductivity and resistance increased with increased pressure, likely because of the decrease in distance between conductive particles. The objects show good response to cyclic loading when taken repeatedly to compressive strains of 25 and 50%. Notably, the printing process necessary to make these functional materials required multiple steps. Firstly, the hydrogel was extruded onto an APS-containing gelatin membrane sacrificial layer, then this printed layer was placed onto a thin layer of PDMS. Hot water was used to remove the gelatin, releasing the APS initiator and resulting in a secondary solidification, and finally the DN hydrogel was encapsulated with another layer of PDMS. Through this process, they printed a sensor to monitor human motion in real time in conjunction with an application they developed for a smartphone.

Cheng and co-workers also used polysaccharide-based hydrogels to create self-healing, dynamic materials.[180] They use Monoamine oxidase B to deaminate benzylamine-functionalized PEG. The corresponding benzaldehyde functionalized PEG after deamination can be crosslinked with amine-containing polysaccharides and proteins such as glycol chitosan and gelatin to form Schiff bases as dynamic bonds. Cheng and co-workers showed that these gels could be extruded, with potential for 3D printing, and that a gel disc could heal from a complete cut in ambient temperature when incubated for 12 h. Connal and co-workers similarly use benzaldehyde functionalized poly(2-hydroxyethyl methacrylate) and ethylenediamine to form self-healing gels with dynamic Schiff base crosslinks, and successfully printed structures using ME.[181] Their gels show 98% recovery from mechanical damages after 12 min in ambient temperature, with thicker printed structures recovering after 1 h.

pH-Dependent Swelling. Melt material extrusion has certain material requirements in order for printing to be successful. The material must be filamentized, generally needs to be linear so that it can melt and flow at high temperatures, have structural integrity when below melt temperature, and have low surface roughness. These requirements have often made the melt extrusion of materials such as hydrogels, and specifically stimuli-responsive hydrogels, not possible, as crosslinking is necessary for the material to be useful. Connal and co-workers have circumvented these limitations through post-crosslinking of their pH-responsive material after filament printing.[182] Through blending of poly(2-vinylpyridine) (P2VP) (which exhibits a globule-to-coil transition upon protonation below pH 4.0) and acrylonitrile-butadiene-styrene, a filament was made and melt extruded into 3D objects. These 3D structures were then post-crosslinked through quaternizing the nitrogen centers of the P2VP to create pH-responsive swellable objects. Future applications of these hydrogel objects could include use as membrane polymers and valves.

Magnetorheological. The use of magnetic particles and magnetic fields in 3D printing processes has the potential to increase the level of control and complexity of outputted 3D objects. Studart and co-workers showed an exciting example of this with the use of magnetic fields in the 3D printing of multi-material composites to control orientation of anisotropic particles. This compositional control, termed by the group as 5D printing, enabled modulation of the mechanical properties and physical responses of printed objects and valves.[183] Recently, Li and co-workers reported the first example of a 3D printed magnetorheological elastomer.[184] Magnetorheological elastomers are a class of smart materials in which damping and elastic properties can be altered by the presence of a magnetic field through the incorporation of ferrous particles into the composite matrix.[185] Li and co-workers used a multi-material extruder printer coupled with UV laser to extrude a carbonyl iron powder/silicone grease mix and encase it within a UV-curable elastomer. They then showed that rheological changes in stiffness, viscous damping coefficient, and peak stress were all increased in the presence of a magnetic field at multiple strain rates. As these materials are made through the incorporation of a viscous fluid within an elastomer, they are known as hybrid fluid-elastomeric magnetorheological materials. The presence of a high viscosity fluid within the elastomer allowed for higher damping capabilities in these printed objects than in existing magnetorheological elastomeric materials. Further exploration by Li and co-workers into the effect of shearing mass and input acceleration suggests that coupling of these factors with magnetic fields may result in even better active vibration control.[186]

Conclusions

This review summarizes the recent advancements in AM enabled by stimuli and AM of stimuli-responsive constructs. Stimuli-responsive materials serve an important role in AM to both enable printing of 3D objects and introduce stimuli-responses downstream of printing. Functional materials for AM is a rapidly expanding field, as represented by the fact that over fifty of the references reported in this review are from the last year alone. Despite the advances in the field, there are still inherent limitations to many AM processes. For example, MME still primarily relies upon linear polymers, and is also prone to defects stemming from lamination issues and differential heating that can lead to a decline in mechanical properties when compared to traditional manufacturing techniques such as injection molding. Incorporation of self-healing, dynamic crosslinking, and self-reinforcing materials into processes like MME could reduce or remove these limitations, while maintaining the benefits of AM such as freedom in object design.

AM of stimuli-responsive materials will enable applications and devices not previously possible. The rate of advancement in fields such as wearable electronics is steadily increasing. This can already be seen in the number of strain, tactile, and force sensors printed within the last year with ease through a multitude of AM processes. Personalized medicine becomes one step closer to reality through AM of stimuli-responsive materials. Photothermally-responsive drug capsules can be printed and modified with ease to help control delivery release and speed. Developments in the AM of organ-on-a-chips can give more insight into an organs response to certain chemicals and stimulants, and responsive implant, stint, and suture designs using SMP's can enable self-fitting devices to reduce surgery and recovery time. Advances in AM of mechanoresponsive and self-healing materials can help visualize and counter the stress on materials in engineering applications, helping to improve their design and overall lifetime.

Despite all of these advances, there is still a lot of room to grow. Just as an AM method can limit the incorporation of stimuli-responsive materials downstream, so too can the extent of available stimuli-responsive materials limit AM. With continued research in increasing the toolbox of printable shear-thinning, thermoresponsive, self-healing, photoresponsive, and other stimuli-responsive materials, AM processes can continue to be improved. As researchers begin to develop and expand this library of accessible stimuli-responsive materials and AM methods, it will be exciting to see how these materials begin to be used towards dynamically responsive objects with multiple stimuli-responses. Complex, responsive, and smart material fabrication is necessary for advancements in manufacturing to continue to match our advancements in computation and theoretical design. AM and stimuli-responsive materials can break the barrier between our imaginations and reality.

Acknowledgements

Financial support from the Army Research Office (Grant No. W911NF-17-1-0595), University of Washington Amazon Catalyst Program (funded by Amazon), and Camille and Henry Dreyfus Foundation. This material is based upon work supported by the National Science Foundation Graduate Research Fellowship Program (JJS) under Grant No. DGE-1256082.

Notes and references

1 T. Wohlers and T. Gornet, *Wohlers Report*, 2014, **24**, 118.
2 B. P. Conner, G. P. Manogharan, A. N. Martof, L. M. Rodomsky, C. M. Rodomsky, D. C. Jordan and J. W. Limperos, *Addit. Manuf.*, 2014, 1, 64-76.
3 W. Gao, Y. Zhang, D. Ramanujan, K. Ramani, Y. Chen, C. B. Williams, C. C. Wang, Y. C. Shin, S. Zhang and P. D. Zavattieri, *Comput. Aided Des.*, 2015, 69, 65-89.
4 A third industrial revolution, The Economist, April, 21st, 2012.
5 D. Hotza, C. M. Gomes and J. Günster, *Adv. Mech. Eng.*, 2014, **6**, 645075. 1
6 J. Chang, J. He, M. Mao, W. Zhou, Q. Lei, X. Li, D. Li, C.-K. Chua and X. Zhao, *Materials*, 2018, **11**, 166.

7 S. A. M. Tofail, E. P. Koumoulos, A. Bandyopadhyay, S. Bose, L. O'Donoghue and C. Charitidis, *Mater. Today*, 2018, **21**, 22–37.
8 N. A. B. Nordin, M. A. B. Johar, M. H. I. B. Ibrahim and O. M. F. bin Marwah, *IOP Conf. Ser.: Mater. Sci. Eng.*, 2017, **226**, 012176.
9 J. Z. Gul, M. Sajid, M. M. Rehman, G. U. Siddiqui, I. Shah, K.-H. Kim, J.-W. Lee and K. H. Choi, *Sci. Technol. Adv. Mater.*, 2018, **19**, 243–262.
10 M. Wehner, R. L. Truby, D. J. Fitzgerald, B. Mosadegh, G. M. Whitesides, J. A. Lewis and R. J. Wood, *Nature*, 2016, **536**, 451–455.
11 D. Han, C. Farino, C. Yang, T. Scott, D. Browe, W. Choi, J. W. Freeman and H. Lee, *ACS Appl. Mater. Interfaces*, 2018, **10**, 17512–17518.
12 R. L. Truby, M. Wehner, A. K. Grosskopf, D. M. Vogt, S. G. M. Uzel, R. J. Wood and J. A. Lewis, *Adv. Mater.,* 2018, **30**, 1706383. 1
13 R. Bogue, *Sensor Review*, 2016, **36**, 333–338.
14 Y. Xu, X. Wu, X. Guo, B. Kong, M. Zhang, X. Qian, S. Mi and W. Sun, *Sensors*, 2017, **17**, 1166.
15 M. Palo, J. Holländer, J. Suominen, J. Yliruusi and N. Sandler, *Expert Rev. Med. Devices*, 2017, **14**, 685–696.
16 L. K. Prasad and H. Smyth, *Drug Dev. Ind. Pharm.*, 2016, **42**, 1019–1031.
17 J. Goole and K. Amighi, *Int. J. of Pharm.*, 2016, **499**, 376–394.
18 M. O. Oyewumi, *J. Biomol. Res. Ther.*, 2015, **4**, 1–3.
19 J. W. Stansbury and M. J. Idacavage, *Dent. Mater.,* 2016, **32**, 54-64.
20 R. Liska, M. Schuster, R. Infu¨ hr, C. Turecek, C. Fritscher, B. Seidl, V. Schmidt, L. Kuna, A. Haase, F. Varga, H. Lichtenegger and J. Stampfl, *J. Coat. Technol. Res.,* 2007, **4**, 505–510.
21 M. Hoffman, *ACS Macro Lett.,* 2014*,* **3***,* 382–386.
22 S. C. Ligon, R. Liska, J. Stampfl, M. Gurr, and R. Mülhaupt, Polymers for 3D printing and customized additive manufacturing. *Chem. Rev.*, 2017, **117**, 10212-10290.
23 A. R. Schultz, P. M. Lambert, N. A. Chartrain, D. M. Ruohoniemi, Z. Zhang, C. Jangu, M. Zhang, C. B. Williams and T. E. Long, *ACS Macro Lett.,* 2014, **3**, 1205-1209.
24 G. I. Peterson, J. J. Schwartz, D. Zhang, B. M. Weiss, M. A. Ganter, D. W. Storti and A. J. Boydston, *ACS Appl. Mater. Interfaces*, 2016, **8**, 29037−2904.
25 K. Obata, A. El-Tamer, L. Koch, U. Hinze and B. N. Chichkov, *Light: Science & Applications*, 2013, **2**, e116.
26 X. Zhou, Y. Hou and J. Lin, *AIP Advances*, 2015, **5**, 030701.
27 M. Emons, K. Obata, T. Binhammer, A. Ovsianikov, B. N. Chichkov and U. Morgner, *Opt. Mater. Express,* 2012, **2**, 942–947.
28 J.-F. Xing, M.-L. Zheng and X.-M. Duan, *Chem. Soc. Rev.*, 2015, **44**, 5031–5039.
29 J. R. Tumbleston, D. Shirvanyants, N. Ermoshkin, R. Janusziewicz, A. R. Johnson, D. Kelly, K. Chen, R. Pinschmidt, J. P. Rolland, A. Ermoshkin, E. T. Samulski and J. M. DeSimone, *Science*, 2015, **347**, 1349-1352.
30 R. Janusziewicza, J. R. Tumblestonb, A. L. Quintanillac, S. J. Mecham and J. M. DeSimone, *Proc. Natl. Acad. Sci. U.S.A.*, 2016, **113**, 11703-11708.
31 M. Chen, Y. Gu, A. Singh, M. Zhong, A. M. Jordan, S. Biswas, L. T. J. Korley, A. C. Balazs and J. A. Johnson, *ACS Cent. Sci.*, 2017, **3**, 124–134.
32 Y. Mao, K. Yu, M. S. Isakov, J. Wu, M. L. Dunn and H. J. Qi. *Sci. Rep.,* 2015, **5**, 13616.
33 H. Bikas, P. Stavropoulos and G. Chryssolouris, *Int. J. Adv. Manuf. Technol.*, 2016, **83**, 389–405.
34 N. Guo and M. C. Leu, *Front. Mech. Eng.*, 2013, **8**, 215–243.
35 S. C. Ligon, R. Liska, J. Stampfl, M. Gurr and R. Mülhaupt, *Chem. Rev.*, 2017, **117**, 10212–10290.
36 S. Shaffer, K. Yang, J. Vargas, M. A. Di Prima and W. Voit, *Polymer*, 2014, **55**, 5969–5979.
37 J. R. Davidson, G. A. Appuhamillage, C. M. Thompson, W. Voit and R. A. Smaldone, *ACS Appl. Mater. Interfaces*, 2016, **8**, 16961-16966.
38 G. A. Appuhamillage, J. C. Reagan, S. Khorsandi, J. R. Davidson, W. Voit, W. and R. A. Smaldone, *Polymer Chemistry*, 2017, **8**, 2087-2092.
39 K. Yang, J. C. Grant, P. Lamey, A. Joshi-Imre, B. R. Lund, R. A. Smaldone and W. Voit, *Adv. Funct. Mater.*, 2017, **17**, 1700318.
40 C. C. Chang, E. D. Boland, S. K. Williams and J. B. Hoying, *J. Biomed. Mater. Res. B Appl. Biomater.*, 2011, **98B**, 160-170.
41 D. M. Kirchmajer, R. Gorkin III and M. in het Panhuis, *J. Mater. Chem. B*, 2015, **3**, 4105-41.
42 J. A. Lewis, *Adv. Funct. Mater*., 2006, **16**, 2193–2204.
43 T. Jungst, W. Smolan, K. Schacht, T. Scheibel and J. Groll, *Chem. Rev*., 2016, **116**, 1496–1539.
44 A. M'Barki, L. Bocquet and A. Stevenson, *Sci. Rep.*, 2017, **7**, 6017.
45 S. Kyle, Z. M. Jessop, S. P. Tarassoli, A. Al-Sabah, and I. S. Whitaker. In *3D Bioprinting for Reconstructive Surgery: Techniques and Applications*, 2017, vol. 1, ch. 9, pp. 173-189.
46 Y. He, F. Yang, H. Zhao, Q. Gao, B. Xia and J. Fu, *Sci. Rep.*, 2016, **6**, 29977.
47 N. Paxton, W. Smolan, T. Böck, F. Melchels, J. Groll and T. Jungst, *Biofabrication*, 2017, **9**, 044107.
48 P. T. Smith, A. Basu, A. Saha and A. Nelson, *Polymer*, DOI:10.1016/j.polymer.2018.01.070.
49 R. A. Barry III, R. F. Shepherd, J. N. Hanson, R. G. Nuzzo, P. Wiltzius and J. A. Lewis, *Adv. Mater.*, 2009, **21**, 2407–2410.
50 L. Ouyang, C. B. Highley, C. B. Rodell, W. Sun and J. A. Burdick, *ACS Biomater. Sci. Eng.*, 2016, **2**, 1743–1751.
51 L. A. Hockaday, K. H. Kang, N. W. Colangelo, P. Y. C. Cheung, B. Duan, E. Malone, J. Wu, L. N. Girardi, L. J. Bonassar, H Lipson, C. C. Chu and J. T. Butcher, *Biofabrication*, 2012, **4**, 035005.
52 A. Sydney Gladman, E. A. Matsumoto, R. G. Nuzzo, L. Mahadevan and J. A. Lewis, *Nat. Mater.*, 2016, **15**, 413–418.
53 A. Lode, F. Krujatz, S. Brüggemeier, M. Quade, K. Schütz, S. Knaack, J. Weber, T. Bley and M. Gelinsky, *Eng. Life Sci.*, 2015, **15**, 177–183.
54 C. B. Highley, C. B. Rodell and J. A. Burdick, *Adv. Mater.*, 2015, **27**, 5075–5079.
55 K. Dubbin, Y. Hori, K. K. Lewis and S. C. Heilshorn, *Adv. Healthc. Mater.*, 2016, **5**, 2488–2492.
56 M.-Y. Yeh, J.-Y. Zhao, Y.-R. Hsieh, J.-H. Lin, F.-Y. Chen, R. D. Chakravarthy, P.-C. Chung, H.-C. Lin and S.-C. Hung, *RSC Adv.*, 2017, **7**, 21252–21257.
57 G.-E. Yu, Y. Deng, S. Dalton, Q.-G. Wang, D. Attwood, C. Price and C. Booth, *J. Chem. Soc., Faraday Trans.*, 1992, **88**, 2537–2544.

58 W. Wu, A. DeConinck and J. A. Lewis, *Adv. Mater.*, 2011, **23**, H178–H183.
59 D. B. Kolesky, R. L. Truby, A. S. Gladman, T. A. Busbee, K. A. Homan and J. A. Lewis, *Adv. Mater.,* 2014, **26**, 3124–3130.
60 T. J. Hinton, Q. Jallerat, R. N. Palchesko, J. H. Park, M. S. Grodzicki, H.-J. Shue, M. H. Ramadan, A. R. Hudson and A. W. Feinberg, *Sci. Adv.,* 2015, **1**, e1500758/1–e1500758/10.
61 A. Basu, A. Saha, C. Goodman, R. T. Shafranek and A. Nelson, *ACS Appl. Mater. Interfaces*, 2017, **9**, 40898–40904.
62 A. Saha, T. G. Johnston, R. T. Shafranek, C. J. Goodman, J. G. Zalatan, D. W. Storti, M. A. Ganter and A. Nelson, *ACS Appl. Mater. Interfaces*, 2018, **10**, 13373–13380.
63 M. Müller, J. Becher, M. Schnabelrauch and M. Zenobi-Wong, *Biofabrication*, 2015, **7**, 035006.
64 M. Zhang, A. Vora, W. Han, R. J. Wojtecki, H. Maune, A. B. A. Le, L. E. Thompson, G. M. McClelland, F. Ribet, A. C. Engler and A. Nelson, *Macromolecules*, 2015, **48**, 6482–6488.
65 D. G. Karis, R. J. Ono, M. Zhang, A. Vora, D. Storti, M. A. Ganter and A. Nelson, *Polym. Chem.*, 2017, **8**, 4199–4206.
66 T. Billiet, E. Gevaert, T. De Schryver, M. Cornelissen and P. Dubruel, *Biomaterials*, 2014, **25**, 49-62.
67 A. L. Rutz , K. E. Hyland , A. E. Jakus, W. R. Burghardt and R. N. Shah, *Adv. Mater.,* 2015, **27**, 1607–1614.
68 H. Meng and G. Li, *Polymer,* 2013, **54**, 2199-2221.
69 D. Ratna and J. Karger-Kocsis, *J. Mater. Sci.,* 2008, **43**, 254-269.
70 J. Hu, Y. Zhu, H. Huang and J. Lu, *Prog. Polym. Sci.,* 2012, **37**, 1720-1763.
71 J. Leng, X. Lan, Y. Liu and S. Du, *Prog. Polym. Sci.,* 2011, **56**, 1077-1135.
72 T. Xie, *Polymer,* 2011, **52**, 4985-5000.
73 3D Insider, http://3dinsider.com/5-most-popular-3d-printing-thermoplastics, (accessed September 2017).
74 J. Raasch, M. Ivey, D. Aldrich, D. S. Nobes and C. Ayranci, *Addit. Manuf.*, 2015, **8**, 132-141.
75 F. S. Senatov, K. V. Niaza, M. Y. Zadorozhnyy, A. V. Maksimkin, S. D. Kaloshkin and Y. Z. Estrin, *J. Mech. Behav. Biomed. Mater.*, 2016, **57**, 139-148.
76 M. Zarek, M. Layani, I. Cooperstein, E. Sachyani, D. Cohn, and S. Magdassi, *Adv. Mater.,* 2016, **28**, 4449-4454.
77 Q. Ge, A. M. Sakhaei, H. Lee, C. K. Dunn, N. X. Fang and M. L. Dunn, *Sci. Rep.,* 2016, **6**, 31110.
78 S. Miao, W. Zhu, N. J. Castro, M. Nowicki, X. Zhou, H. Cui, J. P. Fisher and L. G. Zhang, *Sci. Rep.,* 2016, **6**, 27226.
79 S. Miao, W. Zhu, N. J. Castro, J. Leng and L. G. Zhang, *Tissue Engineering Part C: Methods*, 2016, **22**, 952-963.
80 W. J. Hendrikson, J. Rouwkema, F. Clementi, C. A. Van Blitterswijk, S. Farè and L. Moroni, *Biofabrication*, 2017, **9**, 031001.
81 A. S. Wu, W. Small IV, T. M. Bryson, E. Cheng, T. R. Metz, S. E. Schulze, E. B. Duoss and T. S. Wilson, *Sci. Rep.*, 2017, **7**, 4664.
82 A. T. Clare, P. R. Chalker, S. Davies, C. J. Sutcliffe and S. Tsopanos, *Int. J. Mech. Mater. Des.,* 2008, **4**, 181-187.
83 S. Dadbakhsh, M. Speirs, J. P. Kruth and J. V. Humbeeck, *Manufacturing Technology,* 2015, **64**, 209-212.
84 S. Dadbakhsh, M. Speirs, J. P. Kruth, J. Schrooten, J. Luyten and J. V. Humbeeck, *Adv. Eng. Mater.,* 2014, **16**, 1140-1146.
85 C. Haberland, M. Elahinia, J. M. Walker, H. Meier and J. Frenzel, *Smart Mater. Struct.*, 2014, **23**, 104002.
86 H. Meier, R. Zarnetta, C. Haberland and J. Frenzel, in Innovative Developments in Design and Manufacturing, ed. P. J. S. Bartolo, M. A. Jorge, F. C. Batista, H. A. Almeida, J. M. Matias, J. C. Vasco, J. B. Gaspar, M. A. Correia, N. C. Andre, N. F. Alves, P. P. Novo, P. G. Martinho and R. A. Carvalho, CRC Press, Leiria Portugal, 4th edition, 2009.
87 K. Lu and W. T. Reynolds, *Powder Technology*, 2008, **187**, 11-18.
88 B. Zhang, J. Chen and C. Coddet, *Journal of Science & Technology,* 2013, **29**, 863-867.
89 Y. Liu, J. K. Boyles, J. Genzer and M. D. Dickey, *Soft Matter*, 2012, **8**, 1764-1769.
90 A. Zolfagharian, A. Z. Kouzani, B. Nasri-Nasrabadi, S. Adams, S. Y. Khoo, M. Norton, I. Gibson and A. Kaynak, *KnE Engineering*, 2017, **2**, 15-22.
91 Z. Quan, D. Yan, K. Zhang and G. Hu, *Sci. Rep.,* 2015, **5**, 8936.
92 Z. Quan, K. Zhang and G. Hu, *Sci. Rep.,* 2016, **6**, 22431.
93 Q. Ge, C. K. Dunn, H. J. Qi and M. L. Dunn, *Smart Mater. Struct.,* 2014, **23**, 094007.
94 Q. Ge, H. J. Qi and M. L. Dunn, *Appl. Phys. Lett.,* 2013, **103**, 131901.
95 Z. Ding, C. Yuan, X. Peng, T. Wang, H. J. Qi and M. L. Dunn, *Sci. Adv.*, 2017, **3**, e1602890.
96 H. Wei, Q. Zhang, Y. Yao, L. Liu, Y. Liu and J. Leng, *ACS Appl. Mater. Interfaces,* 2017, **9**, 876.
97 H. Yang, W. R. Leow, T. Wang, J. Wang, J. Yu, K. He, D. Qi, C. Wan and X. Chen, *Adv. Mater.*, 2017, **29**, 1701627.
98 H. Yang, W. R. Leow and X. Chen, *Small Methods*, 2017. doi: 10.1002/smtd.201700259
99 J. N. Rodriguez, C. Zhu, E. B. Duoss, T. S. Wilson, C. M. Spadaccini and J. P. Lewicki, *Sci. Rep.,* 2016, **6**, 27933.
100 D. Raviv, W. Zhao, C. McKnelly, A. Papadopoulou, A. Kadambi, B. Shi, S. Hirsch, D. Dikoysky, M. Zyracki, C. Olguin, R. Raskar and S. Tibbits, *Sci. Rep.,* 2014, **4**, 7422.
101 A. Balasubramanian and C. J. Bettinger, *Adv. Eng. Mater.,* 2015, **17**, 1287-1293.
102 F. S. Senatov, M. Y. Zadorozhnyy, K. V. Niaza, V. V. Medvedev, S. D. Kaloshkin, N. Y. Anisimova, M. V. Kiselevskiy and K. C. Yang, *Eur. Polym. J.*, 2017, **93**, 222-231.
103 M. Bodaghi, A. R. Damanpack and W. H. Liao, *Smart Mater. Struct.,* 2016, **25**, 105034.
104 G. F. Hu, A. R. Damanpack, M. Bodaghi and W. H. Liao, *Smart Mater. Struct.*, 2017, **26**, 125023.
105 M. Bodaghi, A. R. Damanpack and W. H. Liao, *Materials & Design*, 2017, **135**, 26-36.
106 Y. Yang, Y. Chen, Y. Wei and Y. Li, *Int. J. Adv. Manuf. Technol.,* 2016, **84**, 2079-2095.
107 M. D. Monzon, R. Paz, E. Pei, F. Ortega, L. A. Suárez, Z. Ortega, M. E. Alemán, T. Plucinski and N. Clow, *Int. J. Adv. Manuf. Technol.,* 2017, **89**, 1827-1836.
108 M. Zarek, N. Mansour, S. Shapira and D. Cohn, *Macromol. Rapid Commun.*, 2017, **38**, 1600628.
109 A. D. Lantada, A. de Blas Romero and E. C. Tanarro, *Smart Mater. Struct.*, 2016, **25**, 065018.
110 R. Yu, X. Yang, Y. Zhang, X. Zhao, X. Wu, T. Zhao, Y. Zhao and W. Huang, *ACS Appl. Mater. Interfaces,* 2017, **9**, 1820-1829.
111 Y. Y. C. Choong, S. Maleksaeedi, H. Eng, J. Wei and P. C. Su, *Mater. Des.*, 2017, **126**, 219-225.
112 J. Z. Gul, B. S. Yang, Y. J. Yang, D. E. Chang and K. H. Choi, *Smart Mater. Struct.,* 2016, **25**, 115009.
113 H. Li, X. Gao and Y. Luo, *Soft Matter,* 2016, **12**, 3226-3233.
114 S. Chen, Q. Zhang and J. Feng, *J. Mater. Chem. C.,* 2017, **5**, 8361-8365.

115 J. E. M. Teoh, Y. Zhao, J. An, C. K. Chua and Y. Liu, *Smart Mater. Struct.*, 2017, **26**, 125001.
116 J. E. M. Teoh, J. An, C. K. Chua, M. Lv, V. Krishnasamy and Y. Liu, *Virtual and Physical Prototyping*, 2017, **12**, 61-68.
117 J. Wu, C. Yuan, Z. Ding, M. Isakov, Y. Mao, T. Wang, M. L. Dunn and H. J. Qi, *Sci. Rep.,* 2016, **6**, 24224.
118 Y. Mao, Z. Ding, C. Yuan, S. Ai, M. S. Isakov, J. Wu, T. Wang, M. L. Dunn and H. J. Qi. *Sci. Rep.,* 2016, **6**, 24761
119 G. Peterson, M. Larsen, M. Ganter, D. Storti and A. Boydston, *ACS Appl. Mater. Interfaces*, 2015, **7**, 577–583.
120 A. Ramirez, Z. Kean, J. Orlicki, M. Champhekar, S. Elsakr, W. Krause and S. Craig, *Nat. chem.*, 2013, **5**, 757-761.
121 B.Cao, N. Boechler, and A. Boydston, *Polymer*, 2018
122 F. Wang, Y. Chong, F. Wang and C. He, *J. App. Polym. Sci.*, 2017 **134**, 44988.
123 Z. C. Kennedy, D. E. Stephenson, J. F. Christ, T. R. Pope, B. W. Arey, C. A. Barrett and M. G. Warner, *J. Mater. Chem. C.*, 2017, **5**, 9570.
124 G. Villar, A. D. Graham and H. Bayley, *Science*, 2013, **340**, 48.
125 M. J. Booth, V. R. Schild and H. Bayley, *Sci. rep.*, 2017, **7**, 9315.
126 J. L. Connell, E. T. Ritschdorff and J. B. Shear, *Anal. Chem.*, 2016, **88**, 12264-12271.
127 S. Flank, G. E. Ritchie and R. Maksimovic, *3D Print. Addit. Manuf.*, 2015, **2**, 180.
128 Y. L. Kong, I. A. Tamargo, H. Kim, B. N. Johnson, M. K. Gupta, T. W. Koh, H. A. Chin, D. A. Steingart, B. P. Rand and M. C. McAlpine, *Nano Lett.,* 2014. **14**, 7017.
129 M. J. Booth, V. R. Schild, A. D. Graham, S. N. Olof and H. Bayley, *Sci. Adv.*, 2016, **2**, e1600056.
130 M. K. Gupta, F. Meng, B. N. Johnson, Y. L. Kong, L. Tian, Y. W. Yeh, N. Masters, S. Singamaneni and M. C. McAlpine, *Nano Lett.*, 2015, **15**, 5321-5329.
131 C. Ladd, J. H. So, J. Muth and M. D. Dickey, *Adv. Mater.*, 2013, **25**, 5081.
132 D. Espalin, D. W. Muse, E. MacDonald and R. B. Wicker, *Int J Adv Manuf Technol.,* 2014, **72**, 963.
133 C. Shemelya, L. Banuelos-Chacon, A. Melendez, C. Kief, D. Espalin, R. Wicker, G. Krijnen and E. MacDonald, In *SENSORS, 2015 IEEE*, 2015, **1**.
134 S. K. Seol, D. Kim, S. Lee, J. H. Kim, W. S. Chang and J. T. Kim, *Small*, 2015, **11**, 3896.
135 B. W. An, K. Kim, H. Lee, S. Y. Kim, Y. Shim, D. Y. Lee, J. Y. Song and J. U. Park, *Adv. Mater.*, 2015, **27**, 4322.
136 E. Fantino, A. Chiappone, I. Roppolo, D. Manfredi, R. Bongiovanni, C. F. Pirri and F. Calignano, *Adv. Mater.*, 2016, **28**, 3712.
137 H. Ota, S. Emaminejad, Y. Gao, A. Zhao, E. Wu, S. Challa, K. Chen, H. M. Fahad, A. K. Jha, D. Kiriya, W. Gao et al., *Adv. Mater. Technol.*, 2016, **1**, 1600013.
138 J. Vaithilingam, M. Simonelli, E. Saleh, N. Senin, R. D. Wildman, R. J. Hague, R. K. Leach and C. J. Tuck, *ACS Appl. Mater. Interfaces*, 2017, **9**, 6560.
139 S. Sundaram, D. S. Kim, M. A. Baldo, R. C. Hayward and W. Matusik, *ACS Appl. Mater. Interfaces*, 2017, **9**, 32290.
140 Y. Yu, F. Liu and J. Liu, *Rapid Prototyping Journal*, 2017, **23**, 642.
141 Y. Jo, J. Y. Kim, S. Y. Kim, Y. H. Seo, K. S. Jang, S. Y. Lee, S. Jung, B. H. Ryu, H. S. Kim, J. U. Park, Y. Choi and S. Jeong. *Nanoscale*, 2017, **9**, 5072.
142 K. Tian, J. Bae, S. E. Bakarich, C. Yang, R. D. Gately, G. M. Spinks, Z. Suo and J. J. Vlassak, *Adv. Mater.*, 2017, **29**, 1604827.
143 K. Kim, W. Zhu, X. Qu, C. Aaronson, W. R. McCall, S. Chen and D. J. Sirbuly, *ACS Nano*, 2014, **8**, 9799.
144 D. I. Woodward, C. P. Purssell, D. R. Billson, D. A. Hutchins and S. J. Leigh, *Phys. Status Solidi A*, 2015, **212**, 2107.
145 S. J. Leigh, R. J. Bradley, C. P. Purssell, D. R. Billson and D. A. Hutchins, *PloS one*, 2012, **7**, e49365.
146 K. Kim, J. Park, J. H. Suh, M. Kim, Y. Jeong and I. Park, *Sensors and Actuators A: Physical*, 2017, **263**, 493.
147 J. T.Muth, D. M. Vogt, R. L. Truby, Y. Mengüç, D. B. Kolesky, R. J. Wood and J. A. Lewis, *Adv. Mater.*, 2014, **26**, 6307.
148 J. U. Lind, T. A. Busbee, A. D. Valentine, F. S. Pasqualini, H. Yuan, M. Yadid, S. J. Park, A. Kotikian, A. P. Nesmith, P. H. Campbell, J. J. Vlassak, J. A. Lewis and K. K. Parker, *Nat. Mater.*, 2017, **16**, 303.
149 A. D. Valentine, T. A. Busbee, J. W. Boley, J. R. Raney, A. Chortos, A. Kotikian, J. D. Berrigan, M. F. Durstock and J. A. Lewis, *Adv. Mater.*, 2017, 1703817.
150 M. G. Mohammed and R. Kramer, *Adv. Mater.*, 2017, **29**, 1604965.
151 J. Y. Kim, S. Ji, S. Jung, B. H. Ryu, H. S. Kim, S. S. Lee, Y. Choi and S. Jeong, *Nanoscale*, 2017, **9**, 11035.
152 S. Z. Guo, K. Qiu, F. Meng, S. H. Park and M. C. McAlpine, *Adv. Mater.*, 2017, **29**, 1701218.
153 J. H. Kim, W. S. Chang, D. Kim, J. R. Yang, J. T. Han, G. W. Lee, J. T. Kim and S. K. Seol, *Adv. Mater.*, 2015, **27**, 157.
154 C. A. Mandon, L. J. Blum and C. A. Marquette, *Anal. Chem.*, 2016, **88**, 10767.
155 C. A. Mandon, L. J. Blum and C. A. Marquette, *Micromachines*, 2017, **8**, 102.
156 A. Kirillova, R. Maxson, G. Stoychev, C. T. Gomillion and L. Ionov, *Adv. Mater.*, 2017, **29**, 1703443.
157 X. Liu, H. Yuk, S. Lin, G. A. Parada, T.-C. Tang, E. Tham, C. de la Fuente-Nunez, T. K. Lu and X. Zhao, *Adv. Mater.* 2017, 1704821.
158 C. D. Blanchette, J. M. Knipe, J. K. Stolaroff, J. R. DeOtte, J. S. Oakdale, A. Maiti, J. M. Lenhardt, S. Sirajuddin, A. C. Rosenzweig and S. E. Baker, *Nat. Commun.*, 2016, **7**, 11900.
159 A. S. Gladman, E. A. Matsumoto, R. G. Nuzzo, L. Mahadevan and J. A. Lewis, *Nat. Mater.*, 2016, **15**, 413.
160 Y. C. Li, Y. S. Zhang, A. Akpek, S. R. Shin and A. Khademhosseini, *Biofabrication*, 2016, **9**, 012001.
161 X. Wang, Y. Sun, C. Peng, H. Luo, R. Wang and D. Zhang, *ACS Appl. Mater. Interfaces*, 2015, **7**, 26131.
162 F. Momeni, X. Liu and J. Ni, *Mater. Des.*, 2017, **122**, 42.
163 S. E. Bakarich, R. Gorkin, M. I. H. Panhuis and G. M. Spinks, *Macromol. Rapid Commun.*, 2015, **36,** 1211.
164 S. E. Bakarich, R. Gorkin, S. Naficy, R. Gately and G. M. Spinks, *MRS Advances*, 2016, **1**, 521.
165 S. Naficy, R. Gately, R. Gorkin, H. Xin and G. M. Spinks, *Macromol. Mater. Eng.*, 2017, **302**, 1600212.
166 S. E. Bakarich, R. Gorkin, R. Gately, S. Naficy, M. in het Panhuis and G. M. Spinks, *Addit. Manuf.*, 2017, **14**, 24.
167 D. Han, Z. Lu and H. Lee, In *ASME 2016 11th International Manufacturing Science and Engineering Conference* (pp. V001T02A073-V001T02A073). American Society of Mechanical Engineers, 2016, **1**.
168 C. P. Ambulo, J. J. Burroughs, J. M. Boothby, H. Kim, M. R. Shankar and T. H. Ware, *ACS Appl. Mater. Interfaces*, 2017, **9**, 37332-37339.

169 Q. Zhao, Y. Liang, L. Ren, F. Qiu, Z. Zhang and L. Ren, *J. Mech. Behav. Biomed. Mater.*, 2018, **78**, 395.
170 Q. Zhao, L.P. Ning, Y.H. Liang, Z.Z. Zhang and L.Q. Ren, *Polymers*, 2017, **9,** 270.
171 C. Yao, Z. Liu, C. Yang, W. Wang, X.J. Ju, R. Xie and L.Y. Chu, *Adv. Funct. Mater.*, 2015, **25**, 2980.
172 Y. Yang, X. Ding and M. W. Urban, *Prog. Polym. Sci.*, 2015, **49**, 34-59.
173 D. Therriault, S. R. White and J. A. Lewis, *Nat. Mater.*, 2003, **2**, 265-271.
174 K. S. Toohey, N. R. Sottos, J. A. Lewis, J. S. Moore and S. R. White, *Nat. Mater.*, 2007, **6**, 581-585.
175 C. J. Hansen, W. Wu, K. S. Toohey, N. R. Sottos, S. R. White and J. A. Lewis, *Adv. Mater.*, 2009, **21**, 4143-4147.
176 A. R.Hamilton, N. R. Sottos and S. R. White, *Adv. Mater.*, 2010, **22**, 5159-5163.
177 C. J. Hansen, S. R. White, N. R. Sottos and J. A. Lewis, *Adv. Funct. Mater.*, 2011, **21**, 4320-4326.
178 S. Liu and L. Li, *ACS Appl. Mater. Interfaces*, 2017, **9**, 26429-26437.
179 M. A. Darabi, A. Khosrozadeh, R. Mbeleck, Y. Liu, Q. Chang, J. Jiang, J. Cai, Q. Wang, G. Luo and M. Xing, *Adv. Mater.*, 2017, **29**, 1700533.
180 Q. Wei, W. Xu, Q. Zhang, S. Zhang, L. Cheng and Q. Wang, *J. Mater. Chem. B*, 2017, **5**, 5092-5095.
181 M. Nadgorny, Z. Xiao and L. A. Connal, *Mol. Syst. Des. Eng.*, 2017, **2**, 283-292.
182 M. Nadgorny, Z. Xiao, C. Chen and L. A. Connal, *ACS Appl. Mater. Interfaces*, 2016, **8**, 28946-28954.
183 D. Kokkinis, M. Schaffner and A. R. Studart, *Nat. Commun.*, 2015, **6**, 8643.
184 A. K. Bastola, V. T. Hoang and L. Li, *Mater. Des.*, 2017, **114**, 391-397.
185 Y. Li, J. Li, W. Li and H. Du, *Smart Mater. Struct.*, 2014, **23**, 123001.
186 A. K. Bastola, M. Paudel and L. Li, In *ASME 2017 Conference on Smart Materials, Adaptive Structures and Intelligent Systems,* 2017, V001T01A001-V001T01A001. American Society of Mechanical Engineers.